Moonlighting α-PheRS connects JAK/STAT with Notch signaling to modulate intestinal homeostasis

Manh Tin Ho[1], Jiongming Lu[2], Beat Suter[1]

Affiliations:

[1]Institute of Cell Biology, University of Bern, Baltzerstrasse 4, Bern 3012, Switzerland.

[2]Present address: Max Planck Institute for Biology of Ageing, 50931 Köln, Germany.

Corresponding author: beat.suter@izb.unibe.ch

Keywords: aminoacyl tRNA synthetase, Notch signaling, JAK/STAT signaling, stem cell, differentiation, proliferation, intestinal tumor

Author contributions: T.H., J.L. and B.S. conceived the ideas and designed the experiments. T.H. conducted most experiments and performed the analysis of the results. J.L. performed the loss-of-function experiments of PheRS and the mTOR signaling tests, the adult wing measurements and the FACS analysis, including analyzing their data. T.H., J.L. and B.S. wrote the manuscript.

Summary / Abstract

Aminoacyl tRNA synthetases (aaRSs) not only load the appropriate amino acid onto their cognate tRNA, many of them perform additional functions that are not necessarily related to their canonical activities. Phenylalanyl tRNA synthetase (PheRS/FARS) levels are elevated in multiple cancers and, interestingly, also in normal stem cells. Our results show that elevated expression of the α-PheRS subunit stimulates cell proliferation in different tissues, while downregulation of *α-PheRS* reduces organ size. The stimulation of proliferation is independent of the β-PheRS subunit and the aminoacylation activity, and it does not visibly stimulate translation. Furthermore, stem cell-specific overexpression of *α-PheRS* caused a tumor phenotype in the intestine, a phenotype indistinguishable from the *Notch* RNAi phenotype in the same cells. Genetic interactions between *α-PheRS* and *Notch* suggest that their activities neutralize each other and that elevated α-PheRS levels attenuate Notch signaling whether Notch induces differentiation into enterocytes or neuroblast stem cell proliferation. Indeed, in the wing discs system, elevated α-PheRS levels suppress *Notch* transcriptional activity. α-PheRS therefore seems to act as a general regulator of Notch signaling, and its own levels are in turn controlled by Stat92E, the transcription factor of the JAK/STAT signaling pathway that is needed for the differentiation of intestinal stem cells during tissue homeostasis under normal conditions. From this we conclude that the α-PheRS subunit can transmit the activity status of the JAK/STAT pathway to the Notch pathway as a mechanism to coordinate stem cell proliferation with differentiation. In this process, α-PheRS levels balance between tissue development and tissue growth to regulate tissue homeostasis.

55 # Introduction

56 Many cancer tissues display higher levels of Phenylalanyl-tRNA synthetase (PheRS, FARS or
57 FRS) than their healthy counterparts according to the database "Gene Expression across
58 Normal and Tumor tissue" (GENT2; published 2019) (Park et al., 2019). Interestingly, a
59 correlation between tumorigenic events and PheRS expression levels had been noted already
60 much earlier for the development of myeloid leukemia (Sen et al., 1997). Despite this, a
61 possible causative connection between elevated PheRS levels and tumor formation had so far
62 not been reported and, to our knowledge, also not been studied. This might have been due to
63 the assumption that higher PheRS levels could simply reflect the demand of tumorigenic cells
64 for higher levels of translation, or it could have to do with the difficulty of studying the
65 moonlighting function of a protein that is essential in every cell for basic cellular functions
66 such as translation.

67 Aminoacyl-tRNA synthetases (aaRSs) are important enzymes that act by charging
68 transfer RNAs (tRNAs) with their cognate amino acid, a key process for protein translation.
69 This activity makes them essential for accurately translating the genetic information into a
70 polypeptide chain (Schimmel and Soll, 1979). Besides their well-known role in translation, an
71 increasing number of aaRSs have been found to perform additional functions in the cytoplasm,
72 the nucleus and even outside of the cell (Guo and Schimmel, 2013; Nathanson and Deutscher,
73 2000; Smirnova et al., 2012) (Casas-Tinto et al., 2015; Gomard-Mennesson et al., 2007;
74 Greenberg et al., 2008; Otani et al., 2002; Zhou et al., 2014). Moonlighting aaRSs regulate
75 alternative splicing, RNA processing and angiogenesis (Lee et al., 2004). For example, the
76 amino-acid binding site of LysRS has an immune response activity; or TrpRS inhibits the
77 vascular endothelial (VE)-cadherin and through this elicits an anti-angiogenesis activity
78 (Tzima et al., 2005; Yannay-Cohen et al., 2009).

79 Cytoplasmic PheRS is one of the most complex members of the aaRSs family, a
80 heterotetrameric protein consisting of 2 alpha- (α) and 2 beta (β)-subunits responsible for
81 charging $tRNA^{Phe}$ during translation (Roy and Ibba, 2006). The α subunit includes the catalytic
82 core of the tRNA synthetase and the β subunit has structural modules with a wide range of
83 functions, including tRNA anticodon binding, hydrolyzing mis-activated amino acids, and
84 editing misaminoacylated $tRNA^{Phe}$ species (Ling et al., 2007; Lu et al., 2014; Roy and Ibba,
85 2006). Importantly, both subunits are needed for aminoacylation of $tRNA^{Phe}$.

86 We set out to address the question whether and how elevated levels of PheRS can
87 contribute to tumor formation. To test for this activity, we studied the role of PheRS levels in
88 the Drosophila model system with the goal of dissecting the molecular mechanism of such a
89 moonlighting role of *PheRS.* We found that α-PheRS levels regulate cell proliferation, cell
90 differentiation or both in different tissues and cell types. Interestingly, elevated levels of α-
91 PheRS do not simply allow higher levels of translation; α-PheRS performs its moonlighting
92 function by modulating differentiation and proliferation independent of the β-PheRS subunit
93 and aminoacylation activity. Although the consequences of altered levels vary to some degree
94 between tissues, we found that even in two tissues with the most divergent consequences, α-
95 PheRS levels act by repressing the Notch signaling pathway, suggesting that this regulative
96 mechanism is responsible for all moonlighting activities of α-PheRS described here. α-PheRS
97 levels, in turn, are controlled by JAK/STAT signaling in the intestinal system, placing α-PheRS
98 at the intersection between two signaling pathways for the fine tuning of normal tissue
99 homeostasis in the midgut. Focusing on the intestine and intestinal stem cells revealed that
100 elevated α-PheRS levels are tumorigenic in the intestinal model. Given the high demand for
101 research on intestinal diseases and cancer (Markowitz and Bertagnolli, 2009) our work now
102 opens new avenues to test ways to control tissue homeostasis and tumor formation.

103 # Results

104

105 **A non-canonical α-PheRS activity is sufficient to induce additional M-phase cells**

106 To test whether elevated levels of PheRS can stimulate growth or proliferation when other
107 aaRSs are not overexpressed, we overexpressed α-PheRS, β-PheRS, and both subunits together
108 in the posterior compartment (P) of wing discs using the *engrailed-Gal4* (*en-Gal4*) driver. In
109 this assay the anterior compartment expresses normal endogenous levels and serves as an
110 internal control. When α-PheRS was overexpressed in the posterior compartment either alone
111 or together with β-PheRS, the mitotic marker phospho-histone H3 (PH3) revealed a 40%
112 increase in mitotic cells in the posterior (P) compartment relative to the anterior (A) one of the
113 same disc (Fig 1A-C). Because elevated levels of the α-PheRS subunit alone are sufficient for
114 the increase in mitotic cells, this effect is unlikely mediated by increased $tRNA^{Phe}$
115 aminoacylation, which requires both subunits.

116 To test this interpretation, we made a mutant version of α-PheRS in which Tyr412 and
117 Phe438 are replaced by cysteins (Cys). These substitutions are predicted to block the entrance
118 into the phenylalanine binding pocket, preventing binding of Phe and aminoacylation of
119 $tRNA^{Phe}$ by the mutant $PheRS^{Cys}$ (Finarov et al., 2010). To test whether the $PheRS^{Cys}$
120 substitution indeed reduces the aminoacylation activity of PheRS, we expressed mutant and
121 wild-type α-PheRS subunits together with β-PheRS subunits in E. coli, purified them and
122 performed aminoacylation assays. α-$PheRS^{Cys}$ together with wild-type β-PheRS produced the
123 same background signal as the α-PheRS subunit alone, and this signal was clearly lower than
124 the one obtained with wild-type α-PheRS plus β-PheRS (Supplementary Fig S1). The
125 Drosophila cytoplasmic *α-PheRS* gene is localized on the X chromosome. A P-element
126 insertion into the 5'-untranslated region of the α-PheRS transcript (*α-PheRS*^{G2060}) causes

127 recessive lethality that can be rescued by a genomic copy of wild-type *α-PheRS* (*gα-PheRS*)
128 that supports aminoacylation (Lu et al., 2014). A genomic copy of the aminoacylation defective
129 α-*PheRS*^{Cys}, *gα-PheRS*^{Cys} did not rescue the lethality of the *α-PheRS*^{G2060} mutant, indicating
130 that the Cys mutant is indeed not functional in aminoacylation in vivo in Drosophila. Despite
131 this apparently lack of aminoacylation activity, overexpressing a transgenic *α-PheRS*^{Cys} in the
132 posterior compartment of the wing disc also caused a 67% increase in the number of mitotic
133 cells in the above assay (Fig 1C). The fact that the mutant *α-PheRS*^{Cys} version caused an
134 increase in mitotic cells at least as strongly as the wild-type *α-PheRS,* together with the fact
135 that β-PheRS overexpression was not needed for this effect, clearly demonstrates that
136 proliferation can be enhanced without increasing the canonical function of PheRS, suggesting
137 that a non-canonical signal emanating from α-PheRS or α-PheRS^{Cys} is capable of inducing
138 proliferation or over-proliferation.

139 We also tested directly whether PheRS overexpression is unable to cause elevated
140 translation as we expected. For this, we analyzed protein synthesis activity in the two wing
141 compartments by puromycin staining using the ribopuromycylation method (RPM) (Deliu et
142 al., 2017). Overexpression of the transcription factor dMyc increases protein synthesis activity
143 and was therefore used as a positive control for the detection of elevated translation and PMY
144 labeling (Deliu et al., 2017). Indeed, when comparing signal intensity between the posterior
145 and the anterior compartment of the same disc, dMyc overexpression significantly increased
146 the anti-PMY signal in the expressing posterior compartment. In contrast, neither
147 overexpression of α-PheRS alone nor combined with β-PheRS increased the puromycin
148 labeling in the overexpressing compartment (Fig 1D-E'', F). The combined results therefore
149 demonstrate unambiguously that elevated α-PheRS levels cause additional cells to be in mitosis
150 through an aminoacylation- and translation-independent, non-canonical activity. Such elevated
151 α-PheRS levels might specifically slow down progression through M-phase, causing higher

176 activity. It is tempting to speculate that the slightly lower increase in proliferation upon
177 overexpressing the mutant *α-PheRS*^{Cys} (28%) in twin spot clones compared to wild-type *α-*
178 *PheRS* (30%) could be due to reduced translation caused by the overexpression of an inactive
179 α subunit that is predicted to partially act as a dominant negative subunit for the aminoacylation
180 function. If the proliferation function is important for development and homeostasis, reduced
181 *α-PheRS* activity should affect growth and development. Because *α-PheRS* and *β-PheRS* are
182 both essential genes in Drosophila (Lu et al., 2014), we used RNAi to reduce their activity in
183 specific tissues by RNAi (Fig S4A,B). Indeed, knock down in the developing eye reduced the
184 adult eye, whereas knockdown in the larval fat body reduced the size of the entire pupae.
185 Furthermore, RNAi knockdown *α-PheRS* or *β-PheRS* in Kc cells caused these cells to
186 proliferate more slowly than the control cells (Fig S4C). Although it is not clear from these
187 results, which activity of PheRS causes this effect, the phenotypes observed are consistent with
188 a direct function in regulating proliferation.

189

190 **Elevated α-PheRS levels lead to mis-regulation of gut homeostasis by downregulating**
191 **Notch signaling and inhibiting the terminal differentiation of EBs**

192 Tissue growth and homeostasis play important roles in developing and outgrown animals, and
193 they require tight control of stem cell self-renewal and differentiation into daughter cells. The
194 Drosophila midgut is a powerful model to analyze these mechanisms and their interplay.
195 Intestinal stem cells (ISCs) and adult midgut progenitors (AMPs) in the larval gut can either
196 divide asymmetrically or symmetrically (Jiang and Edgar, 2011; Micchelli, 2012). Asymmetric
197 divisions of ISCs give rise to a new ISC and a Su(H)GBE^{+} enteroblast (EB) for the enterocyte
198 (EC) lineage differentiation, or to a pre-enteroendocrine cell (pre-EE) for the enteroendocrine
199 (EE) cell lineage differentiation (Furriols and Bray, 2001; Guo et al., 2016). Differential

152 numbers of cells to remain in the PH3-positive state. Alternatively, they might either promote
153 over-proliferation of mitotic cells or induce proliferation in non-cycling cells.

154

155 **The *α-PheRS* subunit accelerates proliferation in different tissues and its knockdown**
156 **reduces organ size**

157 To test the effects of PheRS levels on proliferation directly and in additional cell types, we set
158 up a mosaic analysis with repressible cell marker (MARCM; (Wu and Luo, 2006) assays in the
159 follicle cells. Twin spot clones were generated with one clone overexpressing PheRS and the
160 GFP marker, and its twin clone expressing normal endogenous levels of PheRS and serving as
161 an internal control (Fig 2A). The results of this experiment showed that clonal overexpression
162 of both subunits of PheRS accelerated the proliferation of the overexpressing cells on average
163 by 32% (Fig 2B). Overexpression of GFP with only the β-PheRS subunit or with GlyRS did
164 not significantly promote clonal expansion (Fig 2B), confirming that the stimulation of growth
165 and proliferation is specific for PheRS and not a general role of aaRSs. Interestingly,
166 overexpression of GFP with the α-PheRS subunit alone also stimulated cell proliferation
167 autonomously by 30% (Fig 2B) and, intriguingly, this was very close to the 32% increase
168 calculated for the clone overexpressing both PheRS subunits (Fig 2B). Remarkably, the higher
169 number of mitotic cells observed upon α-PheRS overexpression in the posterior compartment
170 of the larval wing discs (Fig 1C) was in a comparable range as the proliferation increase in the
171 follicle cell assay (Fig 2B). These results therefore suggest that α-PheRS levels promote cell
172 proliferation and that it has this activity in different tissues.

173 Overexpression of *α-PheRS*^{Cys} alone and *α-PheRS*^{Cys} together with *β-PheRS (PheRS*^{Cys})
174 stimulated clonal growth and cell proliferation in the follicle cell twin spot experiment by 28%
175 and 25%, respectively (Fig 2B), again confirming that this is an aminoacylation-independent

200 Delta/Notch signaling between the ISC and its daughter causes the latter to either differentiate
201 into an absorptive EC lineage or a secretory EE linage by distinct mechanisms (Beehler-Evans
202 and Micchelli, 2015; Micchelli and Perrimon, 2006; Ohlstein and Spradling, 2007; Zeng and
203 Hou, 2015). EBs are intermediate differentiating cells that differentiate into ECs in a Notch-
204 dependent manner (Ohlstein and Spradling, 2006), while the production of EEs has not been
205 molecularly characterized, but the pre-EEs requires only low levels of Notch signaling (Guo et
206 al., 2016). We investigated the effect of overexpression of the *α-PheRS*$^{(Cys)}$ subunit in adult
207 midguts by using the *esg-Gal4*, *tub-Gal80*^{ts}, *UAS-2XEYFP* (referred to as *esg*^{ts}) system
208 (Micchelli and Perrimon, 2006), which allows specific and conditional activation of *α-*
209 *PheRS*$^{(Cys)}$ expression in ISCs and EBs by temperature-shift control. Co-expression of *UAS-*
210 *2XEYFP* allowed us to monitor the activity of the *esg-Gal4* driver. We observed cellular
211 changes in these stem cells as early as 2 days after induction and the phenotypes became more
212 pronounced until day 5, when the elevated α-PheRS$^{(Cys)}$ levels had caused the total numbers of
213 YFP^{+} cells to increase 4.3 fold for the wild type and 4.7 fold for the α-PheRS^{Cys} mutant (Fig
214 S5; Figure 3A-C''',I). This hyperaccumulation of proliferative cells was also accompanied by
215 the formation of tumors composed of ISCs and EBs (Fig 3H). These tumors included
216 proliferating ISCs (YFP^{+}, diploid nuclei) and "differentiating" EBs (YFP^{+}, apparently
217 polyploid nuclei). Differentiating EBs were rarely observed in wild-type midguts (3% of
218 progenitor cells; Fig 3 A-A''',J) and these retained only weak YFP signals. The midgut with
219 high levels of α-PheRS$^{(Cys)}$ showed a significant increase of "differentiating" EBs (20% and
220 22%, respectively, of progenitor cells) and these expressed a strong *esg>YFP* signal (Fig 3B-
221 C''',I,J). Consistent with previous results, the frequency of strong EB tumors was the highest
222 (76%) in the α-PheRS^{Cys} overexpressing guts (Fig 3C-C''',H). In conclusion, elevated α-
223 PheRS$^{(Cys)}$ levels lead to an increase in the numbers of progenitor cells (ISCs and EBs) and

224 tumor formation in the adult midgut, and this phenotype is independent of the aminoacylation
225 activity of PheRS.

226 The increase of the midgut progenitor cells (ISCs and EBs) could be a consequence of
227 a differentiation problem of ISCs (Lian et al., 2018; Mundorf et al., 2019). Indeed, we also
228 observed a change in the ratio of EEs / ECs from 0.1 in the wild type to 0.8 in the *α-PheRS*
229 overexpressing midguts, resulting from counting the cell population in wild type (8% EEs, 68%
230 ECs) and *α-PheRS* overexpressing posterior midguts, which contained 12% EEs and 14% ECs
231 (Figure 3K,L).

232 Several observations indicate that Notch signaling is one of the important signaling
233 pathways for terminal differentiation. We observed that the change in ISC proliferation and
234 EE/EC ratio is similar to the low Notch activity phenotype that had been reported in several
235 studies (Guo and Ohlstein, 2015; Liu et al., 2010; Marianes and Spradling, 2013; Micchelli and
236 Perrimon, 2006; Ohlstein and Spradling, 2007). We confirmed the phenotype by knocking
237 down *Notch* with RNAi treatment with the same esg^{ts} system and confirmed the similarity
238 between Notch knockdown and *α-PheRS* overexpression (Figure 3D-D"',I,L). It is also
239 important to note that the kinetics with which this phenotype developed was the same as for
240 the RNAi knockdown of *N* (Fig S5).

241 We also observed that *α-PheRS* overexpression inhibited the terminal differentiation of
242 progenitors into ECs upon Notch over-activation (Figure 3E-F"'). It has been shown that
243 upregulation of Notch signaling by overexpressing the continuous active form of Notch (Notch
244 intracellular domain – N^{ICD}) would drive ISCs to differentiate into ECs, thereby depleting the
245 ISC pool in wild type adult midguts (Figure 3E-E"') (Micchelli and Perrimon, 2006; Zhai et
246 al., 2017). The overexpression of *α-PheRS* in the Notch over-activation background rescued
247 the ISC pool even beyond the wild type levels (Figure 3F-F"',M). This would also explain the

248 high number of YFP^+ "differentiating" EBs in midguts overexpressing *α-PheRS* alone (Figure
249 3B-B"'). Compared to the wild type EBs, these EBs had a larger cell size and polyploid DNA,
250 indicating that they were in the process of differentiating. The overexpression of *α-PheRS* in
251 these progenitor cells increased the number of "differentiating" EBs by preventing them from
252 undergoing terminal differentiation. Altogether, the high levels of *α-PheRS* induce the ISC and
253 EB tumor phenotype by not only increasing ISC proliferation, but also arresting EBs in their
254 undifferentiated stage.

255 Larval Drosophila midguts possess AMPs as the temporary reserve for adult ISCs.
256 AMPs go through several divisions to form imaginal midgut islets that include AMPs enclosed
257 by a peripheral cell (PC) (Mathur et al., 2010). Due to the transient period of the larval stage,
258 larval midguts do not require EC renewal under normal conditions (Lee and Lee, 2019).
259 However, Houtz et al. reported recently that larval guts can respond to certain damages and
260 injuries by triggering a regenerative process to compensate for depleted ECs in the epithelium
261 and also to allow reconstitution of AMPs (Houtz et al., 2019). We investigated the effect of
262 overexpression of each PheRS subunit in larval AMPs by using the *esg-Gal4, UAS-2XEYFP*
263 driver, which is specifically expressed in AMPs. Co-expression of *UAS-2XEYFP* allowed us
264 to monitor the activity of the *esg-Gal4* driver. The results demonstrated that overexpression of
265 Myc::α-PheRS in the larval midgut significantly increased the proportion of PH3 positive cells
266 (mitotic index) in the posterior midgut (Fig 4A-B', E). Driving the expression of the α-
267 $PheRS^{Cys}$ mutant alone in AMPs also produced a higher mitotic index (Fig 4 C-C',E),
268 indicating again that the aminoacylation function is not required for this activity. Due to lack
269 of epithelial renewal in larval guts, the cell density of larval midguts is usually stable (Lee and
270 Lee, 2019; Mathur et al., 2010). It is therefore surprising that elevated α-PheRS or α-$PheRS^{Cys}$
271 levels increase the cell density in larval midguts (Fig 4F). Altogether, these results showed that

272 elevated α-PheRS$^{(Cys)}$ levels cause AMPs to proliferate and to differentiate, producing
273 additional larval midgut cells.

274 Strikingly, elevated α-PheRS^{Cys} levels induced a tumor phenotype in both anterior and
275 posterior areas of the larval midgut (outlined with white dashed lines, Fig 4C-C') while the
276 overexpression of wild-type Myc::α-PheRS only gave rise to high numbers of AMPs in the
277 posterior larval midgut (Fig 4B-B'). Interestingly, elevated α-PheRS^{Cys} levels also caused the
278 appearance of a more severe tumor phenotype, where individual AMP islets could not be
279 discerned anymore (Fig 4C-C'). Wild-type larval guts contain ECs with large nuclei and
280 interspersed occasional AMP islets with smaller nuclei (as seen in the YFP overexpression
281 control, Fig 4A-A'). In contrast, we observed a phenotype where ECs and AMPs could not be
282 distinguished based on the size of their nuclei, but emerged as a larger cell population with
283 intermediate size nuclei (Fig 4C'). Many of these cells expressed the *esg*>YFP stem cell marker
284 at high levels, but others displayed only a very weak YFP signal. This result is comparable to
285 the EB tumor phenotype in adult midguts where the progenitor cells are prevented from
286 undergoing terminal differentiation (Fig 3 B''',C''',G-G''). In addition, this tumor phenotype
287 was also observed when Notch was downregulated by RNAi using the same induction system
288 (Fig 4D-D'). As seen in Fig 4G, overexpression of *α-PheRS* and *α-PheRS^{Cys}* downregulated
289 the *Notch* activity reporter NRE-eGFP (Notch response element promoter driving the
290 expression of eGFP; (Saj et al., 2010)). This points again to an interaction between α-PheRS
291 and the Notch pathway. We concluded that elevated α-PheRS levels in larval midgut stem cells
292 cause mis-regulation of gut homeostasis, possibly by downregulating Notch signaling and
293 inhibiting the terminal differentiation of the progenitor cells (EBs).

294

295

296 ***α-PheRS* is a novel general repressor of Notch signaling**

297 Developing larval brains contain neuroblasts (NBs), stem cells that divide asymmetrically with
298 one daughter keeping the stemness and the other differentiating into a neuronal cell. Notch
299 signaling plays a crucial role in this process (Ables et al., 2011; Giachino and Taylor, 2014),
300 but in contrast to the situation in the gut, loss of *Notch* prevents NB self-renewal, whereas
301 ectopic expression of *Notch* leads to tumor formation (de la Pompa et al., 1997; Grandbarbe et
302 al., 2003; Hatakeyama et al., 2004). This opposite role of *Notch* makes the NB lineage an ideal
303 complementary system to test whether α-PheRS is a general component of the *Notch* pathway.
304 Driving α-PheRS or the α-PheRS^{Cys} expression in NBs with the *inscutable-Gal4 (incs-Gal4)*
305 driver resulted in significantly smaller central brains (CB), the region where the NBs are
306 located (Fig 5A-A'', B). In contrast, this treatment had little or no effect on the size of the optic
307 lobes (OL). The phenotype was indistinguishable from the phenotype caused by *N* knock-down
308 (Fig 5B), and co-overexpression of *Notch* together with *α-PheRS*^{Cys} in neuroblasts rescued the
309 brains to wild-type size (Fig 5B).

310 Type II neuroblasts are particularly suited to analyze effects on neuroblast
311 differentiation. Targeting specifically the 8 type II neuroblasts in central brain lobes with *α-*
312 *PheRS* or *α-PheRS*^{Cys,} overexpression, resulted in half of the central brains in a strong reduction
313 of the number of neuroblasts, and the resulting central brain lobes ended up smaller (Fig 5 C-
314 F,I). Knocking down *Notch* in type II NBs with RNAi and the same driver combination resulted
315 in a similar phenotype, but with a higher expressivity. On the other hand, overexpression of α-
316 PheRS in type II neuroblasts where *Notch* was also over-activated, partially rescued the tumor
317 phenotype of type II neuroblasts to wild-type numbers and it restored the normal size of the
318 brain (Fig 5G,H). Because the genetic interaction with *Notch* shows that the two activities
319 counteract one another in guts and brains, two tissues where *Notch* has opposing functions on
320 cellular differentiation, it appears that the interaction between *α-PheRS* and *Notch* is not

321 mediated indirectly through a primary effect on division or differentiation, but is likely to be a
322 more direct one. In any case, this interaction appears to modulate tissue homeostasis in different
323 organs.

324 To further address the role of *α-PheRS* on *Notch* signaling, we also studied its effect on
325 the larval wing disc and the adult wing. We investigated the effect of overexpressing *α-PheRS*
326 in adult wings by using the *en-Gal4*, *tub-Gal80*^{ts} (referred to as *en*^{ts}) system. This allowed us
327 to specifically and conditionally activate *α-PheRS*$^{(Cys)}$ expression in the posterior compartment
328 of the wing disc by temperature-shift control. We observed that elevated *α-PheRS* or *α-*
329 *PheRS*^{Cys} levels induced the ectopic vein formation with a new vein branching from the
330 connecting vein between L4 and L5 vein (black arrow head, Fig 6A',A"). Even though the
331 treatment did not cause the appearance of notched wings in our experiment, this ectopic vein
332 phenotype is indistinguishable from the one obtained by downregulating *Notch* by RNAi
333 treatment using the same expression system (Fig 6A"'). This finding suggests that *α-PheRS*
334 might be a more general, novel *Notch* interactor.

335 To test directly for changes in *Notch* activity in response to altered levels of *α-PheRS*
336 or *α-PheRS*^{Cys} in imaginal wing discs, we monitor *Notch* activity with the NRE-eGFP reporter
337 and used the *en-Gal4, tub-Gal80*^{ts}*, UAS-mRFP system to express α-PheRS*$^{(Cys)}$. In this system,
338 *eGFP* expression marks the cells with active Notch signaling along the dorsal ventral (D/V)
339 boundary of the larval wing disc (Fig 6B"). Co-expression of *UAS-mRFP* allowed us to monitor
340 the activity of NRE-eGFP in the posterior compartment of the wing disc (black arrow head,
341 Fig 6B"') while the NRE-eGFP signal in anterior compartment served as an internal wild-type
342 control. In wild-type wing disc, the NRE-eGFP signal is as high in the posterior compartment
343 as in the anterior one (Fig 6C-C"'). As expected, knockdown of *Notch* in the posterior
344 compartment resulted in the exclusion of the eGFP signal from the mRFP-marked posterior
345 compartment (white arrow, Fig 6F-F"'). Importantly, elevated *α-PheRS* or *α-PheRS*^{Cys} levels

346 caused the same loss of eGFP signal in the mRFP-marked posterior compartments (Fig 6D-
347 D''',E-E'''). These observations demonstrated that elevated *α-PheRS* levels downregulate
348 *Notch* activity in larval wing discs. Taken together, the results from midguts, brains and wing
349 discs, demonstrate that *α-PheRS* is a novel general repressor of *Notch* signaling.

350

351 **Transcription factor Stat92E of the JAK/STAT pathway regulates α-PheRS levels**

352 The JAK/STAT signaling pathway is required for the differentiation and maturation of ECs,
353 and knockdown of STAT92E, the transcription factor at the end of the JAK/STAT signaling
354 pathway, results in the formation of EB containing tumors (Zhai et al., 2015). Under normal
355 conditions, STAT92E induces the progenitors to differentiate into ECs via regulating Notch
356 activity (Herrera and Bach, 2019). Under stress conditions, like bacterial infection, secreted
357 Unpaired3 (*Upd3*), a cytokine signal of the JAK/STAT pathway, activates ISC proliferation
358 and differentiation to repair damaged parts of the gut (Buchon et al., 2009; Lin et al., 2010).
359 Upd3 not only activates JAK/STAT signaling in ISCs, but also *Notch* activity to enhance ISC
360 proliferation and to promote differentiation into EC, respectively (Jiang et al., 2009). We
361 therefore tested whether α-PheRS could possibly coordinate JAK/STAT with Notch signaling
362 in adult midguts. Using the hypomorphic $Stat92E^{HJ}$ allele, we tested whether suppressing
363 JAK/STAT signaling affects α-PheRS expression. Indeed, $Stat92E^{HJ}$ mutants displayed
364 elevated levels of α-PheRS in Delta-positive ISCs (Fig 7A-B"). Consistent with this result,
365 *Stat92E* RNAi knock-down under tissue and temporal control also showed elevated α-PheRS
366 levels in ISCs (Fig 7C-C"). As shown in Fig 7D,D', E,E', F,F', G, the levels of α-PheRS
367 significantly increased in ISCs and EBs. The fact that two different approaches to reduce
368 *Stat92E* activity led to higher α-PheRS levels in ISCs and EBs demonstrates that *Stat92E*
369 regulates α-PheRS levels in these cells.

370 Surprisingly, RNAi knock down of *Stat92E* with the *esg*^{ts} system not only affected α-
371 PheRS levels in ISCs, but also in some neighboring polyploid YFP^{-} ECs, but not in distant ECs
372 (arrows in Fig 7C", F-F',G). Because we also observed this phenotype in *Stat92E*^{HJ} mutants
373 (arrows in Fig 7B",E-E',G), this is unlikely to be an off-target effect of the RNAi. It thus
374 appears that either *Stat92E* can normally control α-PheRS levels also in a cell non-autonomous
375 way or α-PheRS levels can be stable longer in YFP^{-} ECs. To test if *Stat92E* is not only required
376 for downregulation of α-PheRS, but also sufficient, we overexpressed *Stat92E* in ISCs and
377 EBs. Indeed, elevated-Stat92E levels reduced the α-PheRS signal in ISCs and EBs (Fig 7H-I").
378 On the other hand, high levels of α-PheRS did not affect *Stat92E* activity when assayed with
379 the *10X STAT92E-GFP* reporter (Bach et al., 2007) that expresses GFP under the control of ten
380 Stat92E binding sites (Fig 7J-K"'). We conclude that *Stat92E* can regulate α-PheRS levels
381 specifically in EBs and ISCs to maintain stem cell homeostasis.

382 If JAK/STAT regulates α-PheRS levels and these regulate Notch activity, this suggests
383 that α-PheRS levels mediate the interaction between these two pathways. To confirm that the
384 modulation of Notch signaling by JAK/STAT is indeed α-PheRS-dependent, we co-
385 overexpressed STAT92E and α-PheRS and tested the Notch activity in adult midguts with the
386 NRE-eGFP reporter. Co-overexpression of *α-PheRS* and *Stat92E* downregulates the *Notch*
387 activity reporter NRE-eGFP (Fig 7M) and also leads to the tumor-like midgut phenotype (Fig
388 7L") like the phenotype of overexpression of *α-PheRS* alone (Fig 3B, 7L'), whereas STAT92E
389 overexpression alone only produces guts with wild-type appearance (Fig 7L"'). Together with
390 the result that α-PheRS regulates Notch signaling, we therefore identified α-PheRS as an
391 intermediate factor that links the JAK/STAT pathway to Notch signaling to modulate gut
392 homeostasis.

393

394 # Discussion and outlook

395 Our work revealed that *PheRS* not only charges tRNAs with their cognate amino acid Phe, but
396 that it also performs moonlighting functions in regulating cell proliferation and differentiation
397 in different tissues. Levels of α-PheRS are critical for these regulative processes and are
398 generally elevated in healthy stem cells compared to differentiated cells. Similarly, many tumor
399 cells show elevated α-PheRS levels compared to their healthy counterparts and a positive
400 correlation between these levels and tumorigenic events had been noted some time ago (Sen et
401 al., 1997). Several circumstantial and direct evidence show that elevated α-PheRS levels do
402 not simply allow higher translational activity to overcome a growth rate restriction imposed by
403 hypothetically limiting levels of PheRS. One, PheRS is unlikely to be rate-limiting for cellular
404 growth because animals with only one copy of *α-PheRS* or *β-PheRS* do not show a phenotype
405 (Lu et al., 2014) and tissue culture cells can be stimulated to grow more rapidly without
406 stimulating the expression of the two PheRS genes (Chen et al., 2003) (Lu et al., 2014). Indeed,
407 directly measuring translational activity *in situ* (Fig 1D-D") showed the same levels of
408 translation whether *α-PheRS* was overexpressed or not. Furthermore, aminoacylation of
409 $tRNA^{Phe}$ requires both subunits to form the tetrameric protein $\alpha_2\beta_2$-PheRS, and overexpression
410 of an aminoacylation-dead *α-PheRS*^{Cys} mutant subunit alone, (without simultaneous
411 overexpression of the β-PheRS subunit) already led to the accumulation of numerous additional
412 dividing cells, closely resembling the phenotype observed when the wild-type gene was
413 expressed in the same way. We therefore conclude that this activity of *α-PheRS* is independent
414 of its $tRNA^{Phe}$ aminoacylation function.

415 The notion that the α-PheRS subunit can be stable and function independently of the β-
416 subunit was surprising because previous results showed that the two subunits were dependent
417 on the presence of the other subunit for their stability (Antonellis et al., 2018; Lu et al., 2014;

418 Xu et al., 2018). Our results now show that this requirement does not apply to all cell types. In
419 young follicle cells, ISCs and possibly other dividing cells, the overexpression of the α-PheRS
420 subunit alone results in higher levels of α-PheRS accumulation and, in particular when elevated
421 levels were induced in gut ISCs and EBs, this produced a strong phenotype. This suggests that
422 the α- and β-PheRS subunits function together in every cell to aminoacylate $tRNA^{Phe}$, but in
423 addition, the α-subunit can be stable in specific cell types, such as stem cells, where it assumes
424 a novel function in regulating cell proliferation and differentiation. Many differentiating cell
425 types then seem to put a system in place that prevents α-PheRS accumulation at high levels
426 and the effects this causes.

427 PheRS is not the only aaRS family member with roles beyond charging tRNAs (Dolde
428 et al., 2014). For instance, MetRS/MRS is capable of stimulating rRNA synthesis (Ko et al.,
429 2000), GlnRS/QRS can block the kinase activity of apoptosis signal-regulating kinase 1
430 (ASK1) (Ko et al., 2001) and a proteolytically processed form of YARS/TyrRS acts as a
431 cytokine (Casas-Tinto et al., 2015; Greenberg et al., 2008). aaRSs are, however, also not the
432 only protein family which evolved to carry out more than one function. In recent years it has
433 become increasingly evident that many if not most proteins have evolved to carry out not only
434 one, but two or more functions, providing interesting challenges to figure out, which of their
435 activities are important for the individual functions of a protein (Dolde et al., 2014).

436 Elevated levels of α-PheRS promote cell proliferation in different cell types. In follicle
437 cells, more cells were produced in the α-PheRS overexpressing clones compared to wild-type
438 clones. In wing discs, more mitotic cells were detected in most areas of the α-PheRS
439 overexpressing compartment. However, overexpression of α-PheRS alone did not cause the
440 formation of a larger wing in the adult, even though this was sufficient to induce additional
441 mitotic cells in larval discs (Fig S2A,B; Fig 1B-C). Co-overexpression of both subunits was

442 needed to cause a small, but significant increase of the wing (Fig S2B). We also found that in
443 this system, elevated PheRS levels primarily affected cell size, whereas proliferation remained
444 controlled or was compensated for (Supplementary data, Fig S2C,D). The different behavior
445 in this system might be caused by the different driver used for these experiments or by the tight
446 organ size control mechanisms of this organ that are capable of compensating for differences
447 in growth and proliferation (Hariharan, 2015; Martin and Morata, 2006). Additionally,
448 reminiscent of its function in neuroblasts, Notch signaling at the D/V boundary region of the
449 wing disc promotes proliferation (de Celis et al., 1996). Interestingly, upon α-PheRS
450 overexpression in this region, not only Notch activity (Fig 6), but also $PH3^{+}$ cells became
451 absent from this region (Fig 1B"), even though they increase in others. We conclude that even
452 in the wing α-PheRS represses Notch signaling, but different regions of the wing disc respond
453 differently, making the wing disc a more complex system to study the responses to elevated α-
454 PheRS levels.

455 The described non-canonical functions of α-PheRS are not only independent of the
456 aaRS activity, they also do not reflect a function in sensing the availability of its enzymatic
457 substrate, Phe, for the major growth controller, the TOR kinase, like the aaRS members TrpRS
458 or LeuRS (Fig S3) (Adam et al., 2018; Bonfils et al., 2012; Han et al., 2012). In the gut tissue,
459 elevated α-PheRS and α-$PheRS^{Cys}$ levels produced 12-14 times as many tumors and these
460 showed mostly a more severe phenotype (Fig 3H). Such tumors were composed of ISCs and
461 differentiating EBs. Similarly, guts also contained 5-8 times as many mitotic cells when α-
462 $PheRS^{(Cys)}$ was overexpressed (Fig 4E). Together, these results strongly suggest, that also in
463 this situation, the higher levels of α-PheRS induced strong cell proliferation.

464 Notch signaling is known to regulate different cellular behaviors during tissue growth
465 in a context-dependent manner. Most prominently, these are proliferation and differentiation

466 control (Henrique and Schweisguth, 2019; Hori et al., 2013). In this study, we presented the
467 effect of α-PheRS on downregulating Notch signaling activity in different tissues. The
468 overexpression of α-PheRS reproduced the classic "vein formation" phenotype in the adult
469 wings caused by loss-of-Notch (Fig 6A-A"') (Johannes and Preiss, 2002) and its elevated levels
470 also downregulated Notch activity at the D/V boundary in wing discs (Fig 6D-E"'). In ovarian
471 follicle cells, the elevated levels of α-PheRS led to an increase in clone size with more cells
472 per clone (Fig 2). This could theoretically also be explained by an inhibitory effect of α-PheRS
473 on Notch activity, because Notch is required for the follicle cells to exit the mitotic cycle and
474 enter the endocycle stage (Lopez-Schier and St Johnston, 2001). Thus, loss of Notch signaling
475 prevents the epithelial cells from switching from the mitotic cell cycle to the endocycle and
476 leads to overproliferation of follicle cells (Deng et al., 2001; Shcherbata et al., 2004) that would
477 be similar to the phenotype of α-PheRS overexpression in follicle cells. In adult midguts, this
478 activity of α-PheRS interfered with normal homeostasis of ISCs by inducing a typical low
479 Notch activity phenotype with many more ISCs, EBs and EEs (Micchelli and Perrimon, 2006;
480 Ohlstein and Spradling, 2007; Zhai et al., 2015). On the other hand, in the larval brain tissue,
481 Notch signaling plays the opposite regulatory role in the control the stem cell (NB)
482 homeostasis. Here *Notch* promotes NB self-renewal, and ectopic expression of N^{ICD} leads to
483 tumor formation (de la Pompa et al., 1997; Grandbarbe et al., 2003; Hatakeyama et al., 2004).
484 Despite this contrary activity of Notch, elevated α-PheRS showed again an inhibitory effect on
485 Notch, preventing NB self-renewal and thereby reducing the size of the brain lobe (Fig 5A-
486 A",B) and rescuing the tumor phenotype caused by ectopic expression of Notch (Fig 5 G,H).
487 Because α-PheRS levels attenuate Notch signaling in different situations where Notch causes
488 different effects, it seems to be a general component of the Notch signaling.

489 The effect of elevated α-PheRS levels is reminiscent of the effect of overexpressing
490 Hairless (H), an antagonist of Notch signaling that directly binds to the Suppressor of Hairless
491 (Su(H)) and inhibits the activation of Notch downstream targets (Brou et al., 1994; Johannes
492 and Preiss, 2002; Maier et al., 1999). The antagonistic inhibitory mechanism of H on the
493 downstream target genes of the Notch signaling pathway might be a paradigm for the
494 mechanism through which α-PheRS might act on the Su(H) complex and switch a fraction of
495 these complexes from an "on" to an "off" state to modulate the activation of the target genes.
496 It will be interesting to test this model.

497 Overexpression of α-PheRS in gut ISCs interfered with cell fate decisions by driving
498 ISC divisions and by keeping EBs in an early differentiation stage. But in addition, it also
499 induced the ISCs to differentiate into EEs. The combination of these effects resulted in a
500 "tumor-like" phenotype, that had been described as the ISC and EB tumor phenotype
501 (Korzelius et al., 2014; Micchelli and Perrimon, 2006; Zhai et al., 2017; Zhai et al., 2015). The
502 large volume of the tumors was attributed not only to the high number of EBs that emerged
503 from the increased ISC proliferation, but also to the large size of EBs that were arrested in their
504 differentiation. The appearance of this phenotype has been reported in situations where a
505 damaged or injured midgut requires a rapid intestinal regeneration after bacterial infection
506 (Zhai et al., 2017). Several studies reported that under such conditions, JAK/STAT signaling,
507 Notch signaling and other factors (e.g. the transcription factor Sox21a) can orchestrate EB
508 differentiation (Jiang and Edgar, 2011; Jiang et al., 2009; Shaw et al., 2010; Zhai et al., 2017).
509 We therefore addressed the possible role of α-PheRS in connecting the JAK/STAT with the
510 Notch signaling pathway.

511 Because *Stat92E* encodes a transcription factor that is required for the
512 differentiation of ISCs (Chen et al., 2016; Zhai et al., 2015), its effect on α-PheRS protein

513 levels could be through a fairly direct interaction between Stat92E and *α-PheRS*, or more
514 indirectly through an alteration cell fate alteration caused by the absence of Stat92E. The latter
515 hypothesis seems unlikely because in wild-type adult midguts, the different cell types show the
516 same levels of α-PheRS when normal guts are stained (Fig 7A",D-D'). This is because *Stat92E*
517 is highly active in ISCs and EBs (mCherry^{+} cells; Fig 7J'-J"') and keeps α-PheRS at the same
518 level as in differentiated cells. We learned this because reduced *Stat92E* activity caused an
519 increase in α-PheRS levels in ISCs and EBs. If the JAK/STAT pathway is capable of
520 controlling cellular α-PheRS levels in the same cell, and because knockdown
521 of *Stat92E* truncates JAK/STAT signaling and leads to a similar phenotype of EB tumors like
522 what we observed upon *a-PheRS* overexpression (Chen et al., 2016; Zhai et al., 2015), it
523 appears that *Stat92E* regulates ISC differentiation by modulating the *α*-PheRS levels.

524 JAK/STAT signaling is known to stimulate progenitor cell differentiation to regulate
525 normal tissue homeostasis (Herrera and Bach, 2019). Under these normal conditions, it also
526 downregulates α-PheRS levels and, consequently, activates Notch signaling at least partially
527 through downregulating α-PheRS levels to promote differentiation of the progenitor cells into
528 ECs. Interestingly, an interplay between the JAK/STAT and the Notch signaling pathways to
529 maintain ISCs homeostasis had been noticed before in regenerating damaged midguts (Jiang et
530 al., 2009). Our work now reveals an unexpected missing link between these two pathways in
531 normal guts and the gut phenotype caused by elevated levels of α-PheRS also points to the
532 importance of controlling and fine tuning its levels. Therefore, regulation of α-PheRS levels
533 links the two signaling pathways and implicates *PheRS* not only in the regulation of cell
534 proliferation, but also in regulating stem cell and tissue homeostasis by connecting two
535 signaling pathways which have drawn considerable attention for cancer research.

536 Stat92E is a transcription factor, but none of the published reports on Stat92E targets
537 lists the *α-PheRS* gene as a possible target (Bina et al., 2010; Muller et al., 2005; Wang et al.,
538 2013). We also inspected the promoter region of *α-PheRS* gene and found that there are some
539 regions with similarities to Stat92E binding motif (TCCnGAA; with n = 3 or 4 giving the
540 highest affinity for Stat92E binding) (Fig S6 A,B) (Rivas et al., 2008; Tsurumi et al., 2011;
541 Yan et al., 1996). The Stat92E potential binding motif 3 that is closest to the 5′ untranslated
542 region is the best candidate with the possibly highest affinity (n =3) (Fig S6 A,B). Future work
543 should analyze whether Stat92E can bind to the *α-PheRS* promoter and regulate *α-PheRS*
544 directly at the transcriptional level or whether it represses *α-PheRS* more indirectly.

545

546 **Relevance of the moonlighting function of α-PheRS for tumor formation**

547 Improper expression of PheRS was suspected long ago to promote carcinogenesis, but
548 till now the mechanisms behind this effect remained unknown. Elevated levels of the human
549 α-PheRS, FARSA, during the development of myeloid leukemia correlate with tumorigenic
550 events (Sen et al., 1997). The GENT2 database published in 2019 describes also strong positive
551 correlations between PheRS subunit levels and tumorigenic events in several tissues and
552 cancers, including colon cancer, which mostly seems to originate from intestinal stem cells
553 (ISCs) (Barker et al., 2009; Park et al., 2019). Modelling the effect of elevated α-PheRS levels
554 in *Drosophila* ISCs and EBs, we found that elevated levels led to over-proliferation of cells
555 with stem cell characteristics and to changes in cell fate, indicating that elevated α-PheRS
556 levels can indeed be a risk factor for tumor formation.

557 Modeling the effects of elevated α-PheRS levels in ISCs revealed that
558 hyperaccumulation of stem cells, a tumor risk, is mediated by high α-PheRS repressing Notch
559 signaling. In mammals, Notch signaling is essential for maintaining the homeostasis of cell

560 proliferation and differentiation (Qiao and Wong, 2009) similar to the function of Notch
561 signaling in the Drosophila gut that is needed to prevent the induction of tumors in the adult
562 midgut (Micchelli and Perrimon, 2006; Ohlstein and Spradling, 2007). Because in human, mis-
563 regulation of Notch signaling in these processes has been suggested to trigger the development
564 of colon cancer, *Notch* has been proposed as a molecular target for cancer therapy (Yin et al.,
565 2010). The results presented here provide new and unexpected insights into the communication
566 between two major signaling pathways involved in gut tumorigenesis and they suggest new
567 opportunities to target these mechanisms.

568 # Materials and Methods

569 ## Key Resources Table

Reagent or Resource	Sources	Identifier	Additional information
Antibodies			
Anti phospho-Histone H3-rabbit	Cell signaling	9701S	1:200 v/v
Anti phospho-Histone H3-mouse	Cell signaling	9706S	1:200 v/v
Anti *α-PheRS*	Genescript	4668	Customized product (1:200 v/v)
Anti *α-PheRS*	Genescript	4669	Customized product (1:200 v/v)
Anti Myc-mouse	Developmental Studies Hybridoma Bank (DSHB)	9E10	Supernatant (1:3 v/v)
Anti Puromycin	DSHB	PMY-2A4	1:100 v/v
Anti Prospero	DSHB	MR1A	1:200 v/v
Anti Delta	DSHB	C594.9B	1:10 v/v
Anti V5 tag-rabbit	Cell signaling	13202	1:200 v/v
Anti Cy3 rabbit	Jackson Immuno Research	115-165-146	1:200 v/v
Anti-rabbit Alexa Flour 488	Molecular Probes	A-11008	1:200 v/v
Anti-rabbit Alexa Flour 488	Molecular Probes	A-11034	1:200 v/v
Anti-mouse Alexa Flour 488	Molecular Probes	A-11029	1:200 v/v
Anti-rabbit Alexa Flour 488	Life technology	A-21206	1:200 v/v
Anti-rabbit Alexa Flour 594	Invitrogen	A-11037	1:200 v/v
Anti-mouse Alexa Flour 594	Molecular Probes	A-11032	1:200 v/v
Anti-mouse Alexa Flour 568	Life technology	A-10037	1:200 v/v
Anti α-tubulin	Abcam	Ab18251	1:1,000 v/v
Anti GFP	ImmunoKontact	042704	1:1,000 v/v
Anti Myc-rabbit	Santa Cruz	Sc-789	A-12 (1:1,000 v/v)
HRP Anti rabbit IgG antibody (Peroxidase)	Vector	PI-1000	1:10,000 v/v
HRP Anti rabbit IgG antibody (Peroxidase)	Vector	PI-2000	1:10,000 v/v

570

Fly stocks and genetics			
α-PheRS^{G2060}/FM6	Bloomington Drosophila Stock Center (BDSC)	26625	
RNAi- α-PheRS	Vienna Drosophila RNAi Center (VDRC)	33514	
RNAi- β-PheRS	VDRC	42046	
gα-PheRS^{Cys}			Transgenic construct
UAS-α-PheRS^{Cys}			Transgenic construct
hspFLP ; Act-Gal4/CyO ; neoFRT82B,tub-Gal80/TM3,Sb			
w ; lf/CyO ; neoFRT82B,UAS- α-PheRS$^{(Cys)}$			
eyeless-Gal4	BDSC	5535	
ppl-Gal4	BDSC	58768	
engrailed-Gal4	BDSC	30564	
engrailed-Gal4,NRE-EGFP,UAS-myrRFP	BDSC	30730	
UAS-GFP	BDSC	6658	
STAT92E[HJ]/TM3,Sb	BDSC	24510	
w; UAS-Myc::MYC	BDSC	9674	
hspFLP/y ; + ; UAS-Myc::MYC	BDSC	9675	
hspFLP/y ; UAS-N^{ICD} /CyO ; MKRS/TM2	BDSC	52008	
10X STAT92E GFP	BDSC	26197	
w,UAS-STAT92E RNAi	BDSC	26899	
NRE-EGFP	BDSC	30727	
UAS-N RNAi	BDSC	7078	
*neoFRT*82B *Sb1*/TM6	BDSC	2051	
NRE-eGFP	BDSC	30728	
UAS-Dl	BDSC	5614	
tub-Gal4/TM3,Sb	BDSC	5138	
w*, Insc-Gal4	BDSC	8751	
w*,UAS-Dicer2 ; wor-Gal4, ase-Gal80; UAS-mCD8::GFP	IMBA		A gift from Juergen A. Knoblich, IMBA
y w att2A[vas-ϕ]; +; attP-86F	ETH Zurich		A gift from Hugo Stocker, ETH
esg-Gal4,UAS-2XEYFP;MKRS/TM6B,Tb	ETH Zurich		A gift from Hugo Stocker, ETH
esg-Gal4,UAS-2XEYFP;tub-Gal80^{ts}/TM3,Sb	ETH Zurich		A gift from Hugo Stocker, ETH
yw; esg-Gal4, UAS-GFP/TM6B,Tb,Hu	ETH Zurich	2400	A gift from Hugo Stocker, ETH
NP1-Gal4 (Myo31DF or Myo1A-Gal4)/CyO, y+	ETH Zurich	2398	A gift from Hugo Stocker, ETH
esg-Gal4, UAS-mCherry-CD8, tub-gal80^{ts}/CyO			A gift from Péter Nagy, Cornell University
UAS-STAT-GFP	Centro Andaluz de Biología del Desarrollo		A gift from Sol Sotillos Martín, Centro Andaluz de Biología del Desarrollo
yw;UAS-cyto-gars-myc/CyO			A gift from Albena Jordanova, VIB-U Antwerp Center for Molecular Neurology

571

Bacteria strains and vectors		
XL1 blue	Aligent	200249
Rosseta – Novagen	Merckmilipore	70954
pET-28a – Novagen	Merckmilipore	69864
pET LIC (2A-T)	Addgene	29665
pUASattB	Drosophila Genomics Resource Center	1419
pw+SNattB	(Koch et al., 2009)	
Commercial assay or kit		
Pierce® Silver Stain kit	Thermo Scientific	24612
Pierce® BCA Protein Assay kit	Thermo Scientific	23227
ReliaPrep™ DNA CleanUp and Concentration System	Promega	A2893
GeneElute™ HP Plasmid miniprep kit	Sigma	NA0160
Qiagen® Plasmid Plus Midi kit	Qiagen	12943
Ni-NTA affinity resin	Qiagen	30210
ECL™ Prime Western Blotting System	GE Healthcare	RPN2232
RNAMaxx™ High Yield Transcription Kit	Aligent	200339
Software, algorithm		
Leica Application Suite X (LAS X)	Leica	https://www.leica-microsystems.com/products/microscope-software/p/leica-las-x-ls/
FIJI	ImageJ	https://fiji.sc/
GraphPad Prism	GraphPad	https://www.graphpad.com/scientific-software/prism/
FlowJo™	BD Biosciences	https://www.flowjo.com/
Microsoft Excel	Microsoft	https://products.office.com/en-us/excel

572

573 **Buffers**

Lysis buffer for Drosophila tissue	**Lysis buffer for bacteria**
20 mM Tris HCl pH7.4 150uM NaCl 2 mM EDTA 50 mM NaF 10% Glycerol 1% Triton X100 1 Protease inhibitor cocktail tablet (Roche-4693159001) 1 mM phenylmethylsulphonyl fluoride	20 mM Tris HCl pH7.4 150uM NaCl 2 mM EDTA 50 mM NaF 10% Glycerol 1% Triton X100 4mM Imidazole 1M 0.6% Lysozyme 1 Protease inhibitor cocktail tablet 1 mM phenylmethylsulphonyl fluoride
4% PFA	**1X PBST**
1X PBST 4% (w/v) Paraformaldehyde	0.2 % (v/v) Tween 20 1X PBS
Blocking buffer	**Fly food recipe**

5% (w/v) non-fat dry milk 0.1% (v/v) Triton X100	20.4 l H_20 1,680 g Maize flour 720 g Yeast 1,800 g Syrup 192 g Potassium sodium tartrate tetrahydrate 36 g Nipagin 120 ml Propionic acid
10X PBS pH 7.4	
10.6 mM KH_2PO_4 1.5 M NaCl 30 mM $Na_2PO_4.7H_20$	
10X SDS running buffer	**10X Transfer buffer**
30 g Tris base 144 g Glycine 10 g SDS dH_2O to 1□	30 g Tris base 144 g Glycine dH_2O to 1□
10X TBS pH to 7.6	**1X TBST**
24 g of Tris Base 88 g of NaCl dH_2O to 1□	100 mL 10X TBS 900 mL dH_2O 0.1% (v/v) Tween 20

574

575 **Primers**

Name	Sequence (5' to 3')	Application
rc2263f	CGCGGATCCATCCGGCGAGAGAGTGTCTTTG	Genomic genomic construct of *α-PheRS*
rc2263r	CGGGGTACCTATGCCTGGCGATAATCGTG	
Tyr412Cys & Phe438Cys-F	TCAAGCCGGCGTACAATCCGTGTACCGAGCCCAG	Construct of *α-PheRS*^{Cys} mutation
Tyr412Cys & Phe438Cys-R	CTCCGGCCGACAGACGCCCGAGTTGCCC	
α-PheRS RNAi 11f	TAATACGACTCACTATAGGGAGGCAAGAAACGCAA GCTCCTC	*α-PheRS* ds RNA synthesis
α-PheRS RNAi 11r	TAATACGACTCACTATAGGGAGGGAACTCCGCCAG ATGTGTG	
β-PheRS RNAi 10f	TAATACGACTCACTATAGGGAGGGCCAATCATTCG GGAATCA	*β-PheRS* ds RNA synthesis
β-PheRS RNAi 10r	TAATACGACTCACTATAGGGAGGAGGCAGGGACTT CTTAATGT	
seq r6	GCTCCCATTCATCAGTTCC	Sequencing
seqA r1	CATTTCCACCGTGAGATCCGTC	Sequencing
seqA r2	AACTCTTGTGGGTGACCGTTTC	Sequencing
seqA f1	GTTCTCGAAGTGAATGTTCTGG	Sequencing
seqA f2	TTTAGCCACCGTCGTCGTTTC	Sequencing
seqA r3	TCCAGCGACGATGACGAATTTG	Sequencing
seqA f3	CAAATGGATTGTGGGACCAGC	Sequencing
seqA r4	GCCCTCCTCCACCATCTTTAG	Sequencing

576

577 **Fly genetics and husbandry**

578 All *Drosophila melanogaster* fly stocks were kept for long term storage at 18ºC in glass or
579 plastic vials on standard food with day/night (12h/12h) light cycles. All experiments were
580 performed at 25ºC unless specifically mentioned. A UAS-GFP element was added in
581 experiments that tested for rescue and involved Gal4 mediated expression of the rescue gene.
582 This construct served to even out the number of UAS sites in each Gal4 expressing cell. Origins
583 of all stocks are noted in the *Key Resource Table*.

584

585 **DNA cloning and generation of transgenic flies**

586 Sequence information was obtained from Flybase. All mutations and the addition of the Myc-
587 tag to the N-terminus of *α-PheRS* were made by following the procedure of the QuickChange®
588 Site-Directed Mutagenesis Kit (Stratagene). The genomic *α-PheRS* rescue construct (*Myc::α-*
589 *PheRS*) codes for the entire coding region and for an additional Myc tag at the N-terminal end.
590 In addition, it contains ~ 1kb of up- and down-stream sequences and it was cloned into the
591 *pw*$^{+}$*SNattB* transformation vector (Koch et al., 2009; Lu et al., 2014). The *α-PheRS* and *β-*
592 *PheRS* cDNAs were obtained by RT-PCR from mRNA isolated from 4-8 days old *OreR* flies
593 (Lu et al., 2014). The Tyr412Cys and Phe438Cys mutations in the *α-PheRS* sequence were
594 created by site directed mutagenesis. Like the wild-type cDNA, they were cloned into the
595 *pUASTattB* transformation vector to generate the pUAS-α-PheRS and pUAS-α-PheRS^{Cys}.
596 Before injecting these constructs into fly embryos, all plasmids were verified by sequencing
597 (Microsynth AG, Switzerland). Transgenic flies were generated by applying the ϕ C31-based
598 integration system with the stock (*y w att2A[vas-ϕ]; +; attP-86F*) (Bischof et al., 2007).

599

600 **Western blotting**

601 Protein was extracted from tissues, whole larvae, or flies using lysis buffer. Protein lysates
602 were separated by SDS-PAGE and transferred onto PVDF membranes (Milipore, US). The
603 blocking was performed for 1h at room temperature (RT) with non-fat dry milk (5%) in TBST
604 solution. Blots were probed first with primary antibodies (diluted in blocking buffer) overnight
605 at 4°C and then with secondary antibodies (diluted in TBST) 1h at RT. The signal of the
606 secondary antibody was detected by using the detect solution mixture (1:1) (ECL™ Prime
607 Western Blotting System, GE Healthcare Life Science) and a luminescent detector (Amersham
608 Imager 600, GE Healthcare Life Science). Origins and recipes of all buffers and reagents are
609 noted in the *Key Resource Table*.

610

611 **Immunofluorescent staining and confocal microscopy**

612 Adult midguts were dissected from each female fly after 5 days at 29°C (unless stated
613 otherwise) or at different time points after 2, 3, 4 days of heat treatment for the time course
614 experiment. A total of 10 guts were analyzed for each genotype. In the larval experiments, the
615 animals were mated at 25°C on fresh, rich diet food and set up for egg laying during a 2 hours
616 window. 120 hours after egg laying, larval midguts were dissected from wandering third instar
617 larvae and a total of 10 guts were analyzed for each genotype. Dissections were performed in
618 PBS 1X on ice and tissues were collected within maximum one hour. Fixation with 4% PFA
619 in PBS-T 0.2% at RT was done for different durations depending on the different tissues: two
620 hours (guts), 40 minutes (brains), 30 minutes (wing discs, ovaries). Then the samples were
621 blocked overnight with blocking buffer at 4°C. Primary antibodies (diluted in blocking buffer)
622 were incubated with the samples for 8h at RT. The samples were rinsed 3 times and washed 3

623 times (20 minutes/wash) with PBST. Secondary antibodies (diluted in PBST) were incubated
624 overnight at 4ºC. The samples were then rinsed 3 times and washed 2 times (20 minutes/wash)
625 with PBST. Hoechst 33258 (2.5 µg/ml) was added in PBST before the last washing step and
626 the samples were mounted with Aqua/Poly Mount solution (Polysciences Inc., US). For the
627 anti-Delta labeling, the samples were blocked for 3h at RT with blocking buffer. The primary
628 anti-Delta antibody (1:10 v/v) was incubated with the samples overnight at 4ºC and then the
629 secondary antibody was incubated overnight at 4ºC. Origins and diluted concentrations of all
630 buffers and antibodies are noted in the *Key Resource Table*.

631

632 **Protein synthesis measurements using the ribopuromycylation method (RPM)**

633 For puromycin labeling experiments, tissues were dissected in Schneider's insect medium
634 (Sigma, US) supplement with 10% fetal calf serum (FCS, Sigma, US) at 25ºC. They were then
635 incubated with Schneider's insect medium containing puromycin (5 µg/ml, Sigma, US) and
636 cycloheximine (CHX, 100 µg/ml, Sigma, US) for 2 hours at RT. Then the samples were fixed
637 with 4% PFA in PBS-T 0.2% at RT and blocked overnight with blocking buffer at 4ºC. Primary
638 anti-Puromycin antibody (diluted in PBST) was incubated with the samples for 8h at RT. The
639 samples were rinsed 3 times and washed 3 times (20 minutes/wash) with PBST. Secondary
640 antibodies (diluted in PBST) were incubated overnight at 4ºC. The samples were then rinsed 3
641 times and washed 2 times (20 minutes/wash) with PBST. Hoechst 33258 (2.5 µg/ml) was added
642 in PBST before the last washing step and the samples were mounted with Aqua/Poly Mount
643 solution (Polysciences Inc., US).

644

645 ***In vitro* aminoacylation assay**

646 Recombinant α-PheRS and β-PheRS proteins were co-expressed in the *E. coli* strain Rosetta
647 (Novagen) and then purified (Moor et al., 2002). For this, the *α-PheRS* or *α-PheRS*^{Cys} mutant
648 cDNAs were cloned with His tags at the N-terminal end into the pET-28a plasmid expression
649 vector (Novagen). Wild-type *β-PheRS* cDNAs were cloned into the pET LIC (2A-T) plasmid
650 (Addgene). Then, His-α-PheRS or the His-α-PheRS^{Cys} mutant and β-PheRS were co-expressed
651 in the *E. coli* strain Rosetta with isopropylthiogalactoside (IPTG, 1mM) induction at 25 °C for
652 6 hours. Proteins were purified with Ni-NTA affinity resin (Qiagen). The aminoacylation assay
653 protocol from Jiongming Lu was then followed (Lu et al., 2014) with the modification that the
654 Whatman filter paper discs were soaked in Phenylalanine solution for 1 hour (30mg/ml in 5%
655 trichloroacetic acid (TCA)) to reduce the background. This assay was performed at 25 °C in a
656 100µl reaction mixture containing 50 mM Tris-HCl pH 7.5, 10 mM $MgCl_2$, 4 mM ATP, 5 mM
657 β-mercaptoethanol, 100 µg/ml BSA, 3 U/ml *E. coli* carrier tRNA, 5 µM [^{3}H]-amino acid (L-
658 Phe) and 1 µM tRNA^{Phe} from brewer's yeast (Sigma, US). In each experiment, a 15-µl aliquot
659 was removed at four different incubation time points, spotted on the Phe-treated Whatman filter
660 paper discs and washed three times with ice-cold 5% TCA and once with ice-cold ethanol. A
661 blank paper disc without spotting and another with spotting the enzyme-free reaction were used
662 for detecting background signals. After filter discs were dried, they were immersed in PPO
663 Toluol (Sigma, US) solution in plastic bottles and the radioactivity was measured by
664 scintillation counting.

665

666 **Wing disc dissociation and FACS analysis**

667 Wandering larvae derived from 2-4 hours egg collections were dissected in PBS during a
668 maximal time of 30 minutes. Around twenty wing discs were incubated with gentle agitation

669 at 29°C for around 2-hours in 500µl 10× Trypsin-EDTA supplemented with 50 µl 10×Hank's
670 Balanced Salt Solution (HBSS) (Sigma, US) and 10 µl Vybrant DyeCycle Ruby stain
671 (Molecular Probes, US). Dissociated cells from wing discs were directly analyzed by FACS-
672 Calibur flow cytometer (Becton Dickinson, US).

673 *Drosophila* tissue culture cells were harvested and fixed in 70% ethanol and stained
674 with a staining solution containing 1mg/ml propidium iodide, 0.1% Triton and 10 mg/ml RNase
675 A. The cells were then subjected to FACS-Calibur cytometry and data were analyzed with the
676 FlowJo software.

677

678 ***Drosophila* cell culture and RNAi treatment**

679 *Drosophila* Kc cells were incubated at 25°C in Schneider's *Drosophila* medium supplemented
680 with 10% heat-inactivated fetal calf serum (FCS) and 50 µg/ml Penicillin/Streptomycin. To
681 induce RNAi knockdown in *Drosophila* cells, dsRNA treatment was performed (Clemens et
682 al., 2000). dsRNAs around 500bp in length were generated with the RNAMaxx™ High Yield
683 Transcription Kit (Agilent, US). Cells were diluted to a concentration of 10^6 cells/ml in serum-
684 free medium, and dsRNA was added directly to the medium at a concentration of 15 µg/ml.
685 The cells were incubated for 1 hour followed by addition of medium containing FCS. Then the
686 cells were kept in the incubator and were harvested at different time points 1-5 days after
687 dsRNA treatment.

688

689 **Clonal assay and twin spot data analysis**

690 For twin spot tests, we used the Mosaic Analysis with a Repressible Cell Marker (MARCM)
691 system. Twin spots were generated with the progenitor genotype *hs-flp; tub-Gal4/UAS-β-*

692 *PheRS ; FRT82B, ubiGFP, UAS-α-PheRS$^{(Cys)}$/FRT82B Tub-Gal80.* In twin spots, the internal
693 control clone was GFP-minus and the twin sister clone produced a red signal by the antibody
694 against the overexpressed protein. We induced the *hs-FLP*, *FRT82B* system at 37°C for 1h on
695 the third day post-eclosure and dissected the animals 3 days post-induction. Confocal imaging
696 detected non-green clones (without ubiGFP) and red clones (stained with Myc antibody-red)
697 (Fig 9A).

698 In twin spots, cell numbers per clone were counted and the numbers of cell divisions
699 per clone were calculated as $\log_2$(cell numbers per clone). This represents the logarithm of the
700 cell numbers per clone to the base 2. The increase of cell proliferation (%) was analyzed by
701 comparing the number of cell divisions of the clone pairs in the same twin spot.

702

703 **Image acquisition and processing**

704 Imaging was carried out with a Leica SP8 confocal laser scanning microscope equipped with
705 a 405 nm diode laser, a 458, 476, 488, 496 and 514 nm Argon laser, a 561 nm diode pumped
706 solid state laser and a 633 nm HeNe laser. Images were obtained with 20x dry and 63x oil-
707 immersion objectives and 1024x1024 pixel format. Images were acquired using LAS X
708 software. The images of the entire gut were obtained by imaging at the standard size and then
709 merging maximal projections of Z-stacks with the Tiles Scan tool. Fluorescent intensity was
710 determined from FIJI software.

711

712 **Quantification of cell numbers per posterior midgut**

713 Z stack images through the width of the posterior midgut were acquired along the length of the
714 posterior midgut from the R4a compartment to the midgut-hindgut junction. Maximum

projections of each Z stack were obtained, and the total number of each cell type were counted manually and exported to Microsoft Excel and GraphPad Prism for further statistical analysis.

Quantification and statistical analysis

For quantifications of all experiments, *n* represents the number of independent biological samples analyzed (the number of guts, the number of wing discs, the number of twin spots), error bars represent standard deviation (SD). Statistical significance was determined using the t-test or ANOVA as noted in the figure legends. They were expressed as P values. (*) denotes $p < 0.05$, (**) denotes $p < 0.01$, (***) denotes $p < 0.001$, (****) denotes $p < 0.0001$. (*ns*) denotes values whose difference was not significant.

Acknowledgements

We thank Peter Nagy, Hugo Stocker, Albena Jordanova, Erik Storkebaum and the Bloomington Stock Center for fly stocks. We are also grateful to Mark Safro for suggesting mutations that disrupt the phenylalanine binding site of α-PheRS. We also thank Rohan Chippalkatti for sharing his knowledge about the larval brain and also Dominique Brunssen and Jonathan Huot for their valuable advices for the aminoacylation assay. This work was supported by the Novartis Foundation for medical-biological Research (#18A050), the Swiss National Fund (project grant 31003A_173188) and the University/Canton of Bern.

References

Ables, J.L., Breunig, J.J., Eisch, A.J., Rakic, P., 2011. Not(ch) just development: Notch signalling in the adult brain. Nature reviews. Neuroscience 12, 269-283.

Adam, I., Dewi, D.L., Mooiweer, J., Sadik, A., Mohapatra, S.R., Berdel, B., Keil, M., Sonner, J.K., Thedieck, K., Rose, A.J., Platten, M., Heiland, I., Trump, S., Opitz, C.A., 2018. Upregulation of tryptophanyl-tRNA synthethase adapts human cancer cells to nutritional stress caused by tryptophan degradation. Oncoimmunology 7, e1486353.

Antonellis, A., Oprescu, S.N., Griffin, L.B., Heider, A., Amalfitano, A., Innis, J.W., 2018. Compound heterozygosity for loss-of-function FARSB variants in a patient with classic features of recessive aminoacyl-tRNA synthetase-related disease. Human mutation 39, 834-840.

Bach, E.A., Ekas, L.A., Ayala-Camargo, A., Flaherty, M.S., Lee, H., Perrimon, N., Baeg, G.H., 2007. GFP reporters detect the activation of the Drosophila JAK/STAT pathway in vivo. Gene expression patterns : GEP 7, 323-331.

Barker, N., Ridgway, R.A., van Es, J.H., van de Wetering, M., Begthel, H., van den Born, M., Danenberg, E., Clarke, A.R., Sansom, O.J., Clevers, H., 2009. Crypt stem cells as the cells-of-origin of intestinal cancer. Nature 457, 608-611.

Beehler-Evans, R., Micchelli, C.A., 2015. Generation of enteroendocrine cell diversity in midgut stem cell lineages. Development 142, 654-664.

Bina, S., Wright, V.M., Fisher, K.H., Milo, M., Zeidler, M.P., 2010. Transcriptional targets of Drosophila JAK/STAT pathway signalling as effectors of haematopoietic tumour formation. EMBO reports 11, 201-207.

Bischof, J., Maeda, R.K., Hediger, M., Karch, F., Basler, K., 2007. An optimized transgenesis system for Drosophila using germ-line-specific phiC31 integrases. Proceedings of the National Academy of Sciences of the United States of America 104, 3312-3317.

Bonfils, G., Jaquenoud, M., Bontron, S., Ostrowicz, C., Ungermann, C., De Virgilio, C., 2012. Leucyl-tRNA synthetase controls TORC1 via the EGO complex. Molecular cell 46, 105-110.

Brou, C., Logeat, F., Lecourtois, M., Vandekerckhove, J., Kourilsky, P., Schweisguth, F., Israel, A., 1994. Inhibition of the DNA-binding activity of Drosophila suppressor of hairless and of its human homolog, KBF2/RBP-J kappa, by direct protein-protein interaction with Drosophila hairless. Genes & development 8, 2491-2503.

Buchon, N., Broderick, N.A., Chakrabarti, S., Lemaitre, B., 2009. Invasive and indigenous microbiota impact intestinal stem cell activity through multiple pathways in Drosophila. Genes & development 23, 2333-2344.

772 Casas-Tinto, S., Lolo, F.N., Moreno, E., 2015. Active JNK-dependent secretion of
773 Drosophila Tyrosyl-tRNA synthetase by loser cells recruits haemocytes during cell
774 competition. Nature communications 6, 10022.

775 Chen, J., Larochelle, S., Li, X., Suter, B., 2003. Xpd/Ercc2 regulates CAK activity and
776 mitotic progression. Nature 424, 228-232.

777 Chen, J., Xu, N., Huang, H., Cai, T., Xi, R., 2016. A feedback amplification loop between
778 stem cells and their progeny promotes tissue regeneration and tumorigenesis. eLife 5.

779 Clemens, J.C., Worby, C.A., Simonson-Leff, N., Muda, M., Maehama, T., Hemmings, B.A.,
780 Dixon, J.E., 2000. Use of double-stranded RNA interference in Drosophila cell lines to
781 dissect signal transduction pathways. Proceedings of the National Academy of Sciences 97,
782 6499-6503.

783 de Celis, J.F., de Celis, J., Ligoxygakis, P., Preiss, A., Delidakis, C., Bray, S., 1996.
784 Functional relationships between Notch, Su(H) and the bHLH genes of the E(spl) complex:
785 the E(spl) genes mediate only a subset of Notch activities during imaginal development.
786 Development 122, 2719-2728.

787 de la Pompa, J.L., Wakeham, A., Correia, K.M., Samper, E., Brown, S., Aguilera, R.J.,
788 Nakano, T., Honjo, T., Mak, T.W., Rossant, J., Conlon, R.A., 1997. Conservation of the
789 Notch signalling pathway in mammalian neurogenesis. Development 124, 1139-1148.

790 Deliu, L.P., Ghosh, A., Grewal, S.S., 2017. Investigation of protein synthesis in Drosophila
791 larvae using puromycin labelling. Biology open 6, 1229-1234.

792 Deng, W.M., Althauser, C., Ruohola-Baker, H., 2001. Notch-Delta signaling induces a
793 transition from mitotic cell cycle to endocycle in Drosophila follicle cells. Development 128,
794 4737-4746.

795 Dolde, C., Lu, J., Suter, B., 2014. Cross Talk between Cellular Regulatory Networks
796 Mediated by Shared Proteins. Advances in Biology 2014, 12.

797 Finarov, I., Moor, N., Kessler, N., Klipcan, L., Safro, M.G., 2010. Structure of human
798 cytosolic phenylalanyl-tRNA synthetase: evidence for kingdom-specific design of the active
799 sites and tRNA binding patterns. Structure 18, 343-353.

800 Furriols, M., Bray, S., 2001. A model Notch response element detects Suppressor of Hairless-
801 dependent molecular switch. Current biology : CB 11, 60-64.

802 Giachino, C., Taylor, V., 2014. Notching up neural stem cell homogeneity in homeostasis and
803 disease. Frontiers in neuroscience 8, 32.

804 Gomard-Mennesson, E., Fabien, N., Cordier, J.F., Ninet, J., Tebib, J., Rousset, H., 2007.
805 Clinical significance of anti-histidyl-tRNA synthetase (Jo1) autoantibodies. Annals of the
806 New York Academy of Sciences 1109, 414-420.

807 Grandbarbe, L., Bouissac, J., Rand, M., Hrabe de Angelis, M., Artavanis-Tsakonas, S.,
808 Mohier, E., 2003. Delta-Notch signaling controls the generation of neurons/glia from neural
809 stem cells in a stepwise process. Development 130, 1391-1402.

810 Greenberg, Y., King, M., Kiosses, W.B., Ewalt, K., Yang, X., Schimmel, P., Reader, J.S.,
811 Tzima, E., 2008. The novel fragment of tyrosyl tRNA synthetase, mini-TyrRS, is secreted to
812 induce an angiogenic response in endothelial cells. FASEB journal : official publication of
813 the Federation of American Societies for Experimental Biology 22, 1597-1605.

814 Guo, M., Schimmel, P., 2013. Essential nontranslational functions of tRNA synthetases.
815 Nature chemical biology 9, 145-153.

816 Guo, Z., Lucchetta, E., Rafel, N., Ohlstein, B., 2016. Maintenance of the adult Drosophila
817 intestine: all roads lead to homeostasis. Current opinion in genetics & development 40, 81-86.

818 Guo, Z., Ohlstein, B., 2015. Stem cell regulation. Bidirectional Notch signaling regulates
819 Drosophila intestinal stem cell multipotency. Science 350.

820 Han, J.M., Jeong, S.J., Park, M.C., Kim, G., Kwon, N.H., Kim, H.K., Ha, S.H., Ryu, S.H.,
821 Kim, S., 2012. Leucyl-tRNA synthetase is an intracellular leucine sensor for the mTORC1-
822 signaling pathway. Cell 149, 410-424.

823 Hariharan, I.K., 2015. Organ Size Control: Lessons from Drosophila. Developmental cell 34,
824 255-265.

825 Hatakeyama, J., Bessho, Y., Katoh, K., Ookawara, S., Fujioka, M., Guillemot, F., Kageyama,
826 R., 2004. Hes genes regulate size, shape and histogenesis of the nervous system by control of
827 the timing of neural stem cell differentiation. Development 131, 5539-5550.

828 Henrique, D., Schweisguth, F., 2019. Mechanisms of Notch signaling: a simple logic
829 deployed in time and space. Development 146.

830 Herrera, S.C., Bach, E.A., 2019. JAK/STAT signaling in stem cells and regeneration: from
831 Drosophila to vertebrates. Development 146.

832 Hori, K., Sen, A., Artavanis-Tsakonas, S., 2013. Notch signaling at a glance. Journal of cell
833 science 126, 2135-2140.

834 Houtz, P., Bonfini, A., Bing, X., Buchon, N., 2019. Recruitment of Adult Precursor Cells
835 Underlies Limited Repair of the Infected Larval Midgut in Drosophila. Cell host & microbe
836 26, 412-425 e415.

837 Jiang, H., Edgar, B.A., 2011. Intestinal stem cells in the adult Drosophila midgut.
838 Experimental cell research 317, 2780-2788.

839 Jiang, H., Patel, P.H., Kohlmaier, A., Grenley, M.O., McEwen, D.G., Edgar, B.A., 2009.
840 Cytokine/Jak/Stat signaling mediates regeneration and homeostasis in the Drosophila midgut.
841 Cell 137, 1343-1355.

842 Johannes, B., Preiss, A., 2002. Wing vein formation in Drosophila melanogaster: hairless is
843 involved in the cross-talk between Notch and EGF signaling pathways. Mechanisms of
844 development 115, 3-14.

845 Ko, Y.G., Kang, Y.S., Kim, E.K., Park, S.G., Kim, S., 2000. Nucleolar localization of human
846 methionyl-tRNA synthetase and its role in ribosomal RNA synthesis. The Journal of cell
847 biology 149, 567-574.

848 Ko, Y.G., Kim, E.Y., Kim, T., Park, H., Park, H.S., Choi, E.J., Kim, S., 2001. Glutamine-
849 dependent antiapoptotic interaction of human glutaminyl-tRNA synthetase with apoptosis
850 signal-regulating kinase 1. The Journal of biological chemistry 276, 6030-6036.

851 Koch, R., Ledermann, R., Urwyler, O., Heller, M., Suter, B., 2009. Systematic functional
852 analysis of Bicaudal-D serine phosphorylation and intragenic suppression of a female sterile
853 allele of BicD. PloS one 4, e4552.

854 Korzelius, J., Naumann, S.K., Loza-Coll, M.A., Chan, J.S., Dutta, D., Oberheim, J., Glasser,
855 C., Southall, T.D., Brand, A.H., Jones, D.L., Edgar, B.A., 2014. Escargot maintains stemness
856 and suppresses differentiation in Drosophila intestinal stem cells. The EMBO journal 33,
857 2967-2982.

858 Lee, J.H., Lee, W.J., 2019. Stealing from the Future: Injured Larvae Spend Stem Cell
859 Deposits. Cell host & microbe 26, 301-303.

860 Lee, S.W., Cho, B.H., Park, S.G., Kim, S., 2004. Aminoacyl-tRNA synthetase complexes:
861 beyond translation. Journal of cell science 117, 3725-3734.

862 Lian, T., Wu, Q., Hodge, B.A., Wilson, K.A., Yu, G., Yang, M., 2018. Drosophila Gut-A
863 Nexus Between Dietary Restriction and Lifespan. International journal of molecular sciences
864 19.

865 Lin, G., Xu, N., Xi, R., 2010. Paracrine unpaired signaling through the JAK/STAT pathway
866 controls self-renewal and lineage differentiation of drosophila intestinal stem cells. Journal of
867 molecular cell biology 2, 37-49.

868 Ling, J., Yadavalli, S.S., Ibba, M., 2007. Phenylalanyl-tRNA synthetase editing defects result
869 in efficient mistranslation of phenylalanine codons as tyrosine. RNA 13, 1881-1886.

870 Liu, J., Sato, C., Cerletti, M., Wagers, A., 2010. Notch signaling in the regulation of stem cell
871 self-renewal and differentiation. Current topics in developmental biology 92, 367-409.

872 Lopez-Schier, H., St Johnston, D., 2001. Delta signaling from the germ line controls the
873 proliferation and differentiation of the somatic follicle cells during Drosophila oogenesis.
874 Genes & development 15, 1393-1405.

875 Lu, J., Bergert, M., Walther, A., Suter, B., 2014. Double-sieving-defective aminoacyl-tRNA
876 synthetase causes protein mistranslation and affects cellular physiology and development.
877 Nature communications 5, 5650.

878 Maier, D., Nagel, A.C., Johannes, B., Preiss, A., 1999. Subcellular localization of Hairless
879 protein shows a major focus of activity within the nucleus. Mechanisms of development 89,
880 195-199.

881 Marianes, A., Spradling, A.C., 2013. Physiological and stem cell compartmentalization
882 within the Drosophila midgut. eLife 2, e00886.

883 Markowitz, S.D., Bertagnolli, M.M., 2009. Molecular origins of cancer: Molecular basis of
884 colorectal cancer. The New England journal of medicine 361, 2449-2460.

885 Martin, F.A., Morata, G., 2006. Compartments and the control of growth in the Drosophila
886 wing imaginal disc. Development 133, 4421-4426.

887 Mathur, D., Bost, A., Driver, I., Ohlstein, B., 2010. A transient niche regulates the
888 specification of Drosophila intestinal stem cells. Science 327, 210-213.

889 Micchelli, C.A., 2012. The origin of intestinal stem cells in Drosophila. Developmental
890 dynamics : an official publication of the American Association of Anatomists 241, 85-91.

891 Micchelli, C.A., Perrimon, N., 2006. Evidence that stem cells reside in the adult Drosophila
892 midgut epithelium. Nature 439, 475-479.

893 Moor, N., Linshiz, G., Safro, M., 2002. Cloning and expression of human phenylalanyl-tRNA
894 synthetase in Escherichia coli: comparative study of purified recombinant enzymes. Protein
895 expression and purification 24, 260-267.

896 Muller, P., Kuttenkeuler, D., Gesellchen, V., Zeidler, M.P., Boutros, M., 2005. Identification
897 of JAK/STAT signalling components by genome-wide RNA interference. Nature 436, 871-
898 875.

899 Mundorf, J., Donohoe, C.D., McClure, C.D., Southall, T.D., Uhlirova, M., 2019. Ets21c
900 Governs Tissue Renewal, Stress Tolerance, and Aging in the Drosophila Intestine. Cell
901 reports 27, 3019-3033 e3015.

902 Nathanson, L., Deutscher, M.P., 2000. Active aminoacyl-tRNA synthetases are present in
903 nuclei as a high molecular weight multienzyme complex. The Journal of biological chemistry
904 275, 31559-31562.

905 Ohlstein, B., Spradling, A., 2006. The adult Drosophila posterior midgut is maintained by
906 pluripotent stem cells. Nature 439, 470-474.

907 Ohlstein, B., Spradling, A., 2007. Multipotent Drosophila intestinal stem cells specify
908 daughter cell fates by differential notch signaling. Science 315, 988-992.

909 Otani, A., Slike, B.M., Dorrell, M.I., Hood, J., Kinder, K., Ewalt, K.L., Cheresh, D.,
910 Schimmel, P., Friedlander, M., 2002. A fragment of human TrpRS as a potent antagonist of
911 ocular angiogenesis. Proceedings of the National Academy of Sciences of the United States
912 of America 99, 178-183.

913 Park, S.J., Yoon, B.H., Kim, S.K., Kim, S.Y., 2019. GENT2: an updated gene expression
914 database for normal and tumor tissues. BMC medical genomics 12, 101.

915 Qiao, L., Wong, B.C., 2009. Role of Notch signaling in colorectal cancer. Carcinogenesis 30,
916 1979-1986.

917 Rivas, M.L., Cobreros, L., Zeidler, M.P., Hombria, J.C., 2008. Plasticity of Drosophila Stat
918 DNA binding shows an evolutionary basis for Stat transcription factor preferences. EMBO
919 reports 9, 1114-1120.

920 Roy, H., Ibba, M., 2006. Phenylalanyl-tRNA synthetase contains a dispensable RNA-binding
921 domain that contributes to the editing of noncognate aminoacyl-tRNA. Biochemistry 45,
922 9156-9162.

923 Saj, A., Arziman, Z., Stempfle, D., van Belle, W., Sauder, U., Horn, T., Durrenberger, M.,
924 Paro, R., Boutros, M., Merdes, G., 2010. A combined ex vivo and in vivo RNAi screen for
925 notch regulators in Drosophila reveals an extensive notch interaction network.
926 Developmental cell 18, 862-876.

927 Schimmel, P.R., Soll, D., 1979. Aminoacyl-tRNA synthetases: general features and
928 recognition of transfer RNAs. Annual review of biochemistry 48, 601-648.

929 Sen, S., Zhou, H., Ripmaster, T., Hittelman, W.N., Schimmel, P., White, R.A., 1997.
930 Expression of a gene encoding a tRNA synthetase-like protein is enhanced in tumorigenic
931 human myeloid leukemia cells and is cell cycle stage- and differentiation-dependent.
932 Proceedings of the National Academy of Sciences of the United States of America 94, 6164-
933 6169.

934 Shaw, R.L., Kohlmaier, A., Polesello, C., Veelken, C., Edgar, B.A., Tapon, N., 2010. The
935 Hippo pathway regulates intestinal stem cell proliferation during Drosophila adult midgut
936 regeneration. Development 137, 4147-4158.

937 Shcherbata, H.R., Althauser, C., Findley, S.D., Ruohola-Baker, H., 2004. The mitotic-to-
938 endocycle switch in Drosophila follicle cells is executed by Notch-dependent regulation of
939 G1/S, G2/M and M/G1 cell-cycle transitions. Development 131, 3169-3181.

940 Smirnova, E.V., Lakunina, V.A., Tarassov, I., Krasheninnikov, I.A., Kamenski, P.A., 2012.
941 Noncanonical functions of aminoacyl-tRNA synthetases. Biochemistry. Biokhimiia 77, 15-
942 25.

943 Tsurumi, A., Xia, F., Li, J., Larson, K., LaFrance, R., Li, W.X., 2011. STAT is an essential
944 activator of the zygotic genome in the early Drosophila embryo. PLoS genetics 7, e1002086.

945 Tzima, E., Reader, J.S., Irani-Tehrani, M., Ewalt, K.L., Schwartz, M.A., Schimmel, P., 2005.
946 VE-cadherin links tRNA synthetase cytokine to anti-angiogenic function. The Journal of
947 biological chemistry 280, 2405-2408.

948 Wang, H., Chen, X., He, T., Zhou, Y., Luo, H., 2013. Evidence for tissue-specific Jak/STAT
949 target genes in Drosophila optic lobe development. Genetics 195, 1291-1306.

950 Wu, J.S., Luo, L., 2006. A protocol for mosaic analysis with a repressible cell marker
951 (MARCM) in Drosophila. Nature protocols 1, 2583-2589.

952 Xu, Z., Lo, W.S., Beck, D.B., Schuch, L.A., Olahova, M., Kopajtich, R., Chong, Y.E.,
953 Alston, C.L., Seidl, E., Zhai, L., Lau, C.F., Timchak, D., LeDuc, C.A., Borczuk, A.C., Teich,
954 A.F., Juusola, J., Sofeso, C., Muller, C., Pierre, G., Hilliard, T., Turnpenny, P.D., Wagner,
955 M., Kappler, M., Brasch, F., Bouffard, J.P., Nangle, L.A., Yang, X.L., Zhang, M., Taylor,
956 R.W., Prokisch, H., Griese, M., Chung, W.K., Schimmel, P., 2018. Bi-allelic Mutations in
957 Phe-tRNA Synthetase Associated with a Multi-system Pulmonary Disease Support Non-
958 translational Function. American journal of human genetics 103, 100-114.

959 Yan, R., Small, S., Desplan, C., Dearolf, C.R., Darnell, J.E., Jr., 1996. Identification of a Stat
960 gene that functions in Drosophila development. Cell 84, 421-430.

961 Yannay-Cohen, N., Carmi-Levy, I., Kay, G., Yang, C.M., Han, J.M., Kemeny, D.M., Kim,
962 S., Nechushtan, H., Razin, E., 2009. LysRS serves as a key signaling molecule in the immune
963 response by regulating gene expression. Molecular cell 34, 603-611.

964 Yin, L., Velazquez, O.C., Liu, Z.J., 2010. Notch signaling: emerging molecular targets for
965 cancer therapy. Biochemical pharmacology 80, 690-701.

966 Zeng, X., Hou, S.X., 2015. Enteroendocrine cells are generated from stem cells through a
967 distinct progenitor in the adult Drosophila posterior midgut. Development 142, 644-653.

968 Zhai, Z., Boquete, J.P., Lemaitre, B., 2017. A genetic framework controlling the
969 differentiation of intestinal stem cells during regeneration in Drosophila. PLoS genetics 13,
970 e1006854.

971 Zhai, Z., Kondo, S., Ha, N., Boquete, J.P., Brunner, M., Ueda, R., Lemaitre, B., 2015.
972 Accumulation of differentiating intestinal stem cell progenies drives tumorigenesis. Nature
973 communications 6, 10219.

974 Zhou, J.J., Wang, F., Xu, Z., Lo, W.S., Lau, C.F., Chiang, K.P., Nangle, L.A., Ashlock,
975 M.A., Mendlein, J.D., Yang, X.L., Zhang, M., Schimmel, P., 2014. Secreted histidyl-tRNA
976 synthetase splice variants elaborate major epitopes for autoantibodies in inflammatory
977 myositis. The Journal of biological chemistry 289, 19269-19275.

978

979

980

981 **Figure legends:**

982

983 **Figure 1: *α–PheRS* overexpression promotes appearance of mitotic cells without *β-PheRS***
984 **and without stimulating translation.**

985 (A-B'''),C) Wing disc phenotypes induced by the overexpression of α-*PheRS* or α-*PheRS*^{Cys}.
986 *en-Gal4 (en-Gal4/+;UAS-GFP/UAS-α-PheRS*$^{(Cys)}$*)* was used to drive transgene expression in
987 the posterior compartment of developing wing discs. Mitotic cells were visualized with anti-
988 phospho-Histone H3 (PH3) antibodies (A: Anterior compartment/P: Posterior compartment).
989 n=10, *p<0.05, **p<0.01 in t-test. (D-E",F) Protein synthesis did not increase upon
990 overexpression of *α-PheRS* or *α-PheRS* and *β-PheRS* together. *en-Gal4* was used to drive the
991 overexpression of the transgenes in the posterior compartment of wing discs. dMyc was used
992 as positive control *(en-Gal4/UAS-Myc::MYC;UAS-GFP/+)*. Protein synthesis was measured
993 by the mean intensity of the puromycin (PMY) signal labelling the nascent polypeptides. n=15,
994 ****p<0.0001, *ns:* not significant.

995

996 **Figure 2: *α-PheRS* levels promote follicle cell proliferation independent of tRNA^{Phe}**
997 **aminoacylation.**
998 Clonal twin spot analysis of the effect of overexpression of the PheRS subunits in follicle cells
999 by the MARCM technique *(hspFLP/+;Act-Gal4/+;neoFRT82B,tub-Gal80/neoFRT82B,UAS-*
1000 *α-PheRS*$^{(Cys)}$*)*. Upon inducing mitotic recombination by a heat-shock (37ºC for 40 minutes), a
1001 recombining cell will divide and give rise to two proliferating clones. (A) One clone (red)
1002 overexpresses PheRS and its twin clone (GFP^{-}) does not and expresses normal levels (internal
1003 control, outlined with yellow line). (B) Three days after inducing the recombination, the
1004 average number of cell divisions were calculated for each clone and compared to its twin spot
1005 to obtain the proliferation increase (%). n= 30, **p<0.01, ***p<0.001, ****p<0.0001 in
1006 ANOVA test.

1007

1008 **Figure 3: Elevated α-PheRS levels lead to mis-regulation of gut homeostasis by**
1009 **attenuating Notch signaling and EB differentiation.**
1010 (A-C''') Overexpression of *α-PheRS* or *α-PheRS*^{Cys} using the *esg-Gal4,UAS-2XEYFP;tub-*
1011 *Gal80*^{ts} (hereby as *esg*^{ts}) system led to an increase in the number of YFP^{+} positive cells and
1012 also induced the formation of ISC and EB tumors *(esg-Gal4,UAS-2XEYFP/+;tub-*
1013 *Gal80*^{ts}*/UAS-α-PheRS*$^{(Cys)}$*)*. (D-D''') Knockdown of *Notch* (*N*) with the same *esg*^{ts} system led
1014 to a similar phenotype as *α-PheRS* overexpression *(UAS-N*^{RNAi}*/+;esg-Gal4,UAS-*
1015 *2XEYFP/+;tub-Gal80*^{ts}*/+)*. (E-F''') Overexpression of *α-PheRS* rescued the depleted ISC pool
1016 caused by Notch over-activation. (G-G",H) Color coded quantification of ISC and EB tumor
1017 frequency by a tumor grading system that is based on the level of accumulating ISCs and EBs.
1018 (I,J) Quantification of YFP^{+} cell numbers and percentage of differentiating EBs among YFP^{+}
1019 cells (A-D''). (K,L) Quantification of the EE/EC ratio and the percentage of the individual cell
1020 type as part of the total number of gut cells of the posterior midgut region analyzed (A-D''').
1021 (M) Quantification of YFP^{+} cell numbers in the experiments (B-B''',E-F'''). In all experiments,
1022 EEs were visualized with the anti-Prospero antibody, YFP^{-}/Hoechst^{+} polyploid cells were
1023 counted as ECs. Animals were mated at 18ºC and adults of the required genotypes were

1024 collected and shifted to 29ºC to inactivate Gal80^{ts}. Adult midguts were dissected from female
1025 flies after 5 days at 29ºC. At least 10 guts were analyzed for each genotype. n=10, **p<0.01,
1026 ***p<0.001, ****p<0.0001 in ANOVA test.

1027

1028 **Figure 4: Elevated α-PheRS leads to a *Notch* knockdown-like phenotype in larval guts.**

1029 (A-D) Whole gut images and (A'-D') pictures of the posterior midgut area (white square). The
1030 expression of the different genes indicated was driven by the *esg-Gal4,UAS-2XEYFP* system.
1031 The YFP displayed in green marks AMPs and EBs, Hoechst (blue) stains the DNA in the nuclei.
1032 Overexpression of the *α-PheRS^{Cys}* mutant gave rise to tumor-like areas in both the anterior and
1033 the posterior midgut (outlined with dashed lines) (*esg-Gal4,UAS-2XEYFP/+;UAS-α-*
1034 *PheRS$^{(Cys)}$/+)*.. (E) Mitotic cells were identified with anti-phospho-Histone H3 (PH3)
1035 antibodies. n=10, ****p<0.0001 in t-test. (F) Total cells per intestinal region were measured
1036 by counting Hoechst 33258 labeled cells manually. n=10, **p<0.01,****p<0.0001. (G) Notch
1037 activity reporter (NRE-eGFP) expresses GFP under the control of a Notch response element
1038 (NRE). The eGFP reporter signal drastically decreases upon *α-PheRS* or *α-PheRS^{Cys}*
1039 overexpression in adult midgut ISCs (*esg-Gal4,UAS-2XEYFP/+;tub-Gal80^{ts}/UAS-α-*
1040 *PheRS$^{(Cys)}$,NRE-eGFP)*. Female flies were collected 3 days after eclosure and cultured at 29ºC
1041 for 5 days before dissecting and harvesting their midguts. Protein lysates were then extracted
1042 and separated by SDS-PAGE gel. 25 guts were analyzed for each genotype.

1043

1044 **Figure 5: High levels of *α-PheRS* repress neuroblast proliferation by downregulating the**
1045 ***Notch* pathway.**

1046 (A-A") The overexpression of *α-PheRS* or *α-PheRS^{Cys}* in neuroblasts reduced the ratio
1047 central brain (CB) size. The *insc-Gal4,UAS-GFP* system was used to overexpress proteins in
1048 neuroblasts (NBs) (*w*, Insc-Gal4/UAS-GFP;UAS-α-PheRS$^{(Cys)}$/+)*. NBs were labelled by
1049 GFP expression. The central brain is shown on the right side (area with GFP^{+} NBs and
1050 outlined by white dashed lines) and the optic lobe areas on the left. (B) Effect of
1051 overexpression of *α-PheRS$^{(Cys)}$*and *N^{ICD},* and *N* knock-down on the CB/OL size ratio. n=20,
1052 ***p<0.001, *ns*: not significant. (C-H, I) Elevated *α-PheRS* or *α-PheRS^{Cys}* levels reduced the
1053 number of Type II NBs per brain lobe, and less than half of the lobes contained the normal 7-
1054 8 NBs. *Notch RNAi* caused the same phenotype with higher expressivity. Overexpressing *α-*
1055 *PheRS^{Cys}* rescued the tumor phenotype caused by ectopic Notch activation in NB to normal
1056 wild-type levels. The larval brains were dissected from third instar larvae, and at least 20
1057 brains were analyzed for each genotype (*w*,UAS-Dicer2/+;wor-Gal4,ase-Gal80/+;UAS-*
1058 *mCD8::GFP/UAS-α-PheRS$^{(Cys)}$)*. Each brain lobe was classified according to the number of
1059 Type II NBs per brain lobe. n = 25.

1060

1061 **Figure 6: Elevated α-PheRS induces ectopic vein formation in adult wings and**
1062 **downregulates Notch activity in wing discs.**

1063 (A-A"') The ectopic wing venation phenotype resulting from elevated levels of α-PheRS or α-
1064 PheRS^{Cys} are similar to the phenotype of *N^{RNAi}* treatment. An ectopic vein branches from the

1065 connecting vein between L4 and L5 vein (arrowhead). Knockdown of *Notch* shows this
1066 phenotype and the classical notched phenotype in the distal region of L3,L4 and near the L5
1067 vein. The *en-Gal4,tub-Gal80^{ts}* (hereby *en^{ts}*) system was used to drive transgene expression in
1068 the posterior compartment of developing wing discs *(en-Gal4/+;tub-Gal80^{ts}/UAS-α-*
1069 *PheRS$^{(Cys)}$)*. Animals were initially kept at 18°C for 3 days and then shifted to 29°C to inactivate
1070 Gal80^{ts} until adult flies eclosed, enabling expression of α-PheRS or α-PheRS^{Cys} or the *N^{RNAi}*.
1071 (B) Schematic illustration of wild-type wing imaginal discs including the different
1072 compartments (left: anterior, right: posterior, up: ventral, down: dorsal), (B') the expression
1073 domain of *en^{ts}*>mRFP and (B") the expression domain of *NRE-eGFP along the ventral/dorsal*
1074 *(V/D) boundary*. (B"')*en-Gal4,NRE-eGFP,UAS-mRFP;tub-Gal80^{ts}* was used to drive
1075 transgene expression in the posterior compartment of developing wing discs and to evaluate
1076 the Notch activity with the reporter *NRE-eGFP* (black arrowhead) *(w,UAS-Dcr2;en-*
1077 *Gal4,UAS-myrRFP,NRE-eGFP/+;tub-Gal80^{ts}/UAS-α-PheRS$^{(Cys)}$)*. (C-F"') Elevated α-PheRS
1078 or α-PheRS^{Cys} leads to the loss of NRE-eGFP expression in the posterior compartments, similar
1079 to the phenotype of *Notch* knockdown *(w,UAS-Dcr2/UAS-N^{RNAi};en-Gal4,UAS-myrRFP,NRE-*
1080 *eGFP/+;tub-Gal80^{ts}/+)*. After egg laying and being kept at 18°C for 6 days, the animals were
1081 shifted to 29°C for 1 day to inactivate Gal80^{ts} and to enable expression of α-PheRS, α-PheRS^{Cys}
1082 or of *N^{RNAi}*.

1083

1084 **Figure 7: The JAK/STAT transcription factor Stat92E regulates α-PheRS levels.**

1085 (A-C'') Hypomorphic *Stat92E^{HJ}* mutants contain elevated levels of α-PheRS in their ISCs (B).
1086 Anti-Delta antibody was used to label ISCs, and anti-α-PheRS was used to stain for α-PheRS.
1087 *esg^{ts}* was used to drive YFP expression in A-A'' (control: *esg-Gal4,UAS-2XEYFP/+;tub-*
1088 *Gal80^{ts}/+)* and in C-C'' (*Stat92E* RNAi: *UAS-Stat92E RNAi/+;esg-Gal4,UAS-2XEYFP/+;tub-*
1089 *Gal80^{ts}/+)*, respectively. YFP therefore marks ISCs and EBs. The white arrows in C", E, F
1090 indicate apparently polyploid YFP^{-} ECs with high levels of α-PheRS. (D-F') Quantification of
1091 the signals along the line in the images D-F (high power pictures of the region outlined in
1092 A,B,C) is based on the lines drawn across the nuclei. Reduced *Stat92E* (hypomorphic allele or
1093 RNAi treatment), showing higher α-PheRS levels in ISCs and EBs when *Stat92E* activity is
1094 reduced. (G) The signal intensity of α-PheRS differs between the ISCs/EBs (YFP^{+} cells), where
1095 it is high, and the distant ECs (white asterisk in C-C", YFP^{-} cells), where it is low, whereas the
1096 signal intensity of α-PheRS is similarly high between the ISCs/EBs and the neighboring ECs.
1097 Lowered JAK/STAT signaling (*Stat92E^{HJ}* allele or by RNAi) significantly elevated the levels
1098 of α-PheRS in ISCs/EBs and neighboring ECs (Nb EC), but not in distant ECs. α-PheRS levels
1099 were measured by the mean intensity of the fluorescent signal. n=10, ****p<0.0001, *ns:* not
1100 significant. (H-I'') Overexpression of *Stat92E* decreased α-PheRS levels in Esg^{+} cells (circled
1101 with white dashed lines) in adult guts *(esg-Gal4,UAS-2XEYFP/UAS-Stat92E-GFP;tub-*
1102 *Gal80^{ts}/+)*. The same imaging settings were used as in (A). (J-K''') As measured by the *10X*
1103 *Stat92E-GFP* reporter, *Stat92E* activity did not alter upon overexpression of *α-PheRS*. The *esg-*
1104 *Gal4,UAS-mCD8:mCherry,tub-Gal80^{ts} system* was used to overexpress *α-PheRS* in ISCs and
1105 EBs *(esg-Gal4,UAS-mCD8:mCherry,tub-Gal80^{ts}/10X Stat92E-GFP;UAS-α-PheRS$^{(Cys)}$/+)*.
1106 Female flies were collected 3 days after eclosure and cultured at 29°C for 5 days before
1107 dissecting and harvesting their midguts. (L-L"') The co-overexpression of *Stat92E* and *α-*
1108 *PheRS* caused the over-proliferative phenotype that is indistinguishable from the *α-PheRS*

overexpression alone phenotype obtained with the *esg-Gal4* driver, whereas the *Stat92E* overexpression alone did not alter the Esg^+ cell numbers. (M) The Notch activity reporter (NRE-eGFP) readout drastically decreased upon overexpression of *α-PheRS* alone *(esg-Gal4,UAS-2XEYFP/+;tub-Gal80^{ts}/UAS-α-PheRS$^{(Cys)}$,NRE-eGFP)*or *Stat92E* and *α-PheRS* co-overexpression *(esg-Gal4,UAS-2XEYFP/UAS-Stat92E-GFP;tub-Gal80^{ts}/UAS-α-PheRS$^{(Cys)}$,NRE-eGFP)*, whereas *Stat92E* overexpression alone increased Notch activity in adult midguts *(esg-Gal4,UAS-2XEYFP/UAS-Stat92E-GFP;tub-Gal80^{ts}/NRE-eGFP)*. Female flies were collected 3 days after eclosure and cultured at 29ºC for 5 days before dissecting and harvesting their midguts. Protein lysates were then extracted and separated by SDS-PAGE gel. 25 guts were analyzed for each genotype.

Figure 1

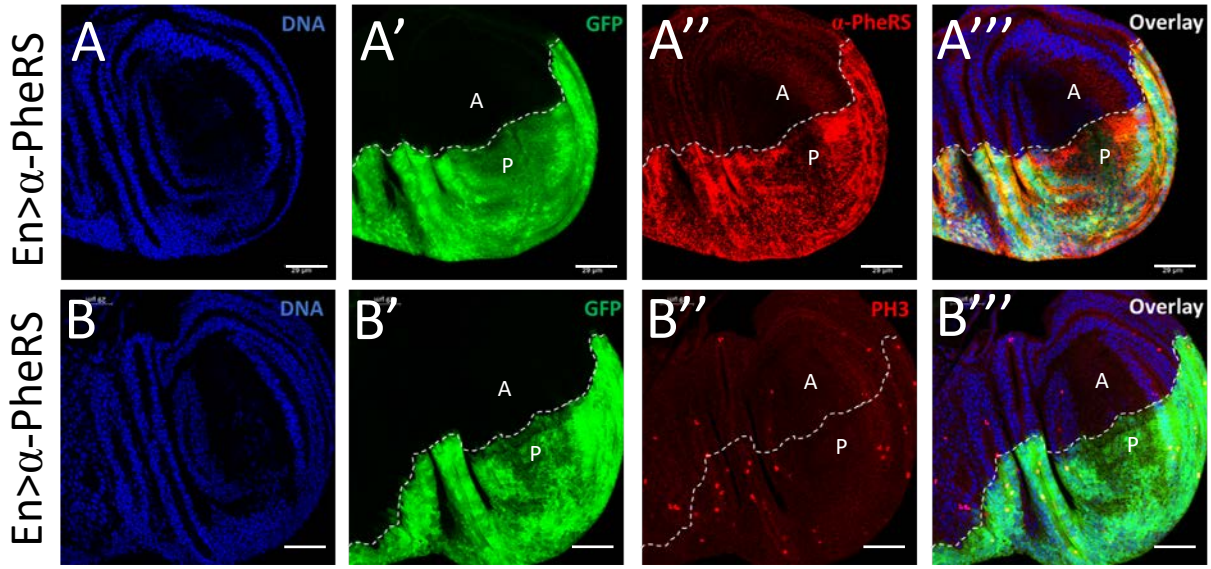
En>α-PheRS
A
DNA
A'
GFP
A''
α-PheRS
A'''
Overlay
A
P
En>α-PheRS
B
DNA
B'
GFP
B''
PH3
B'''
Overlay

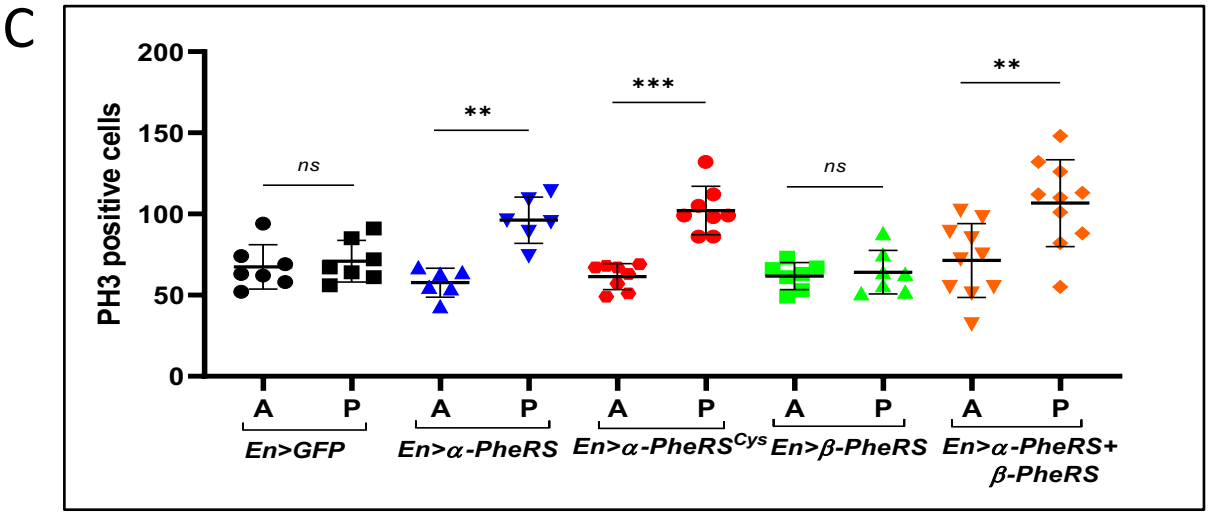
C
PH3 positive cells
200
150
100
50
0
ns
**
***
ns
**
A
P
En>GFP
En>α-PheRS
En>α-PheRS^Cys
En>β-PheRS
En>α-PheRS+ β-PheRS

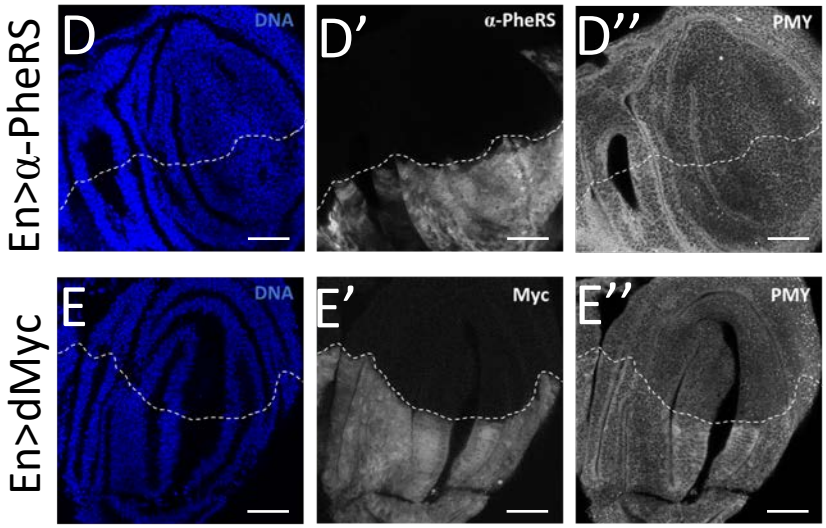
En>α-PheRS
D
DNA
D'
α-PheRS
D''
PMY
En>dMyc
E
DNA
E'
Myc
E''
PMY

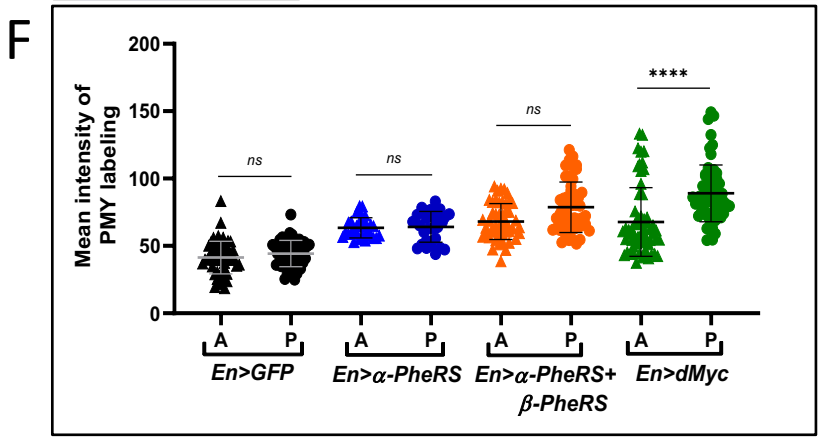
F
Mean intensity of PMY labeling
200
150
100
50
0
ns
ns
ns
****
A
P
En>GFP
En>α-PheRS
En>α-PheRS+ β-PheRS
En>dMyc

Figure 2

A

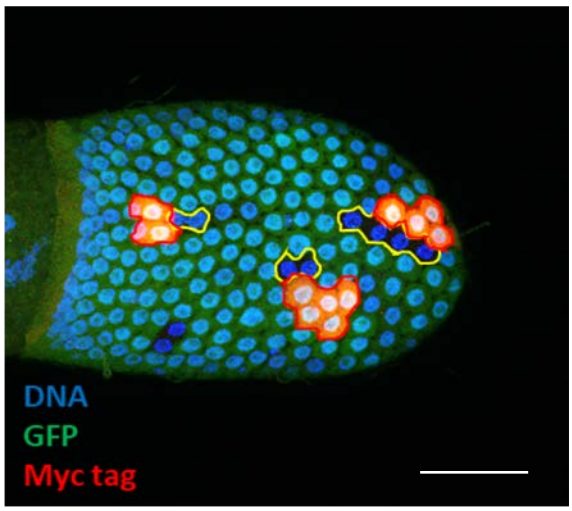
DNA
GFP
Myc tag

B

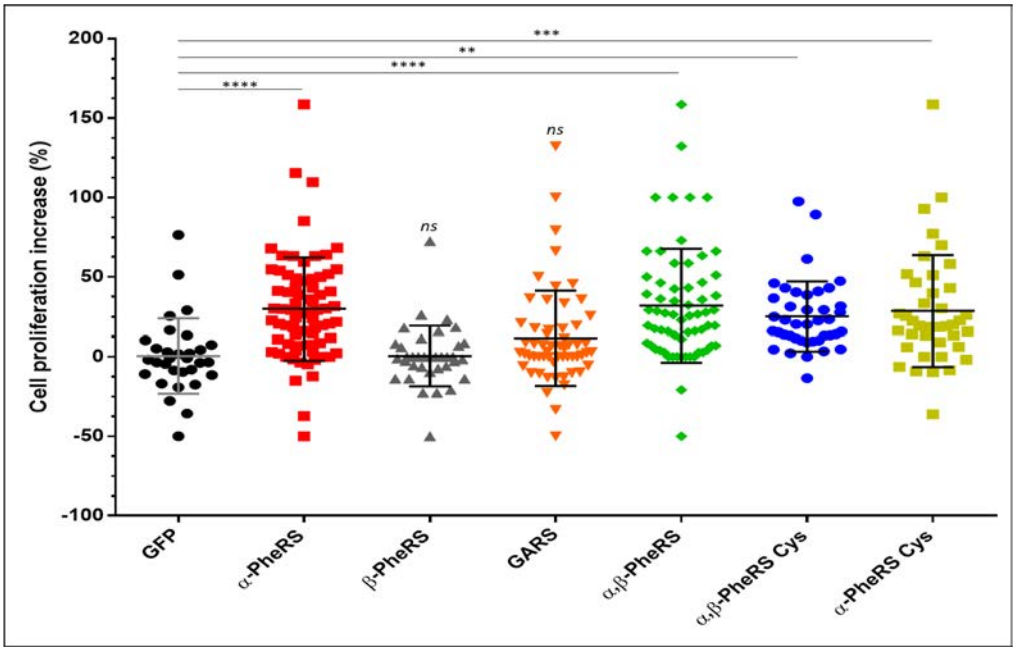
Cell proliferation increase (%)
200
150
100
50
0
-50
-100
***
**
****
****
ns
ns
GFP
α-PheRS
β-PheRS
GARS
α,β-PheRS
α,β-PheRS Cys
α-PheRS Cys

Figure 3

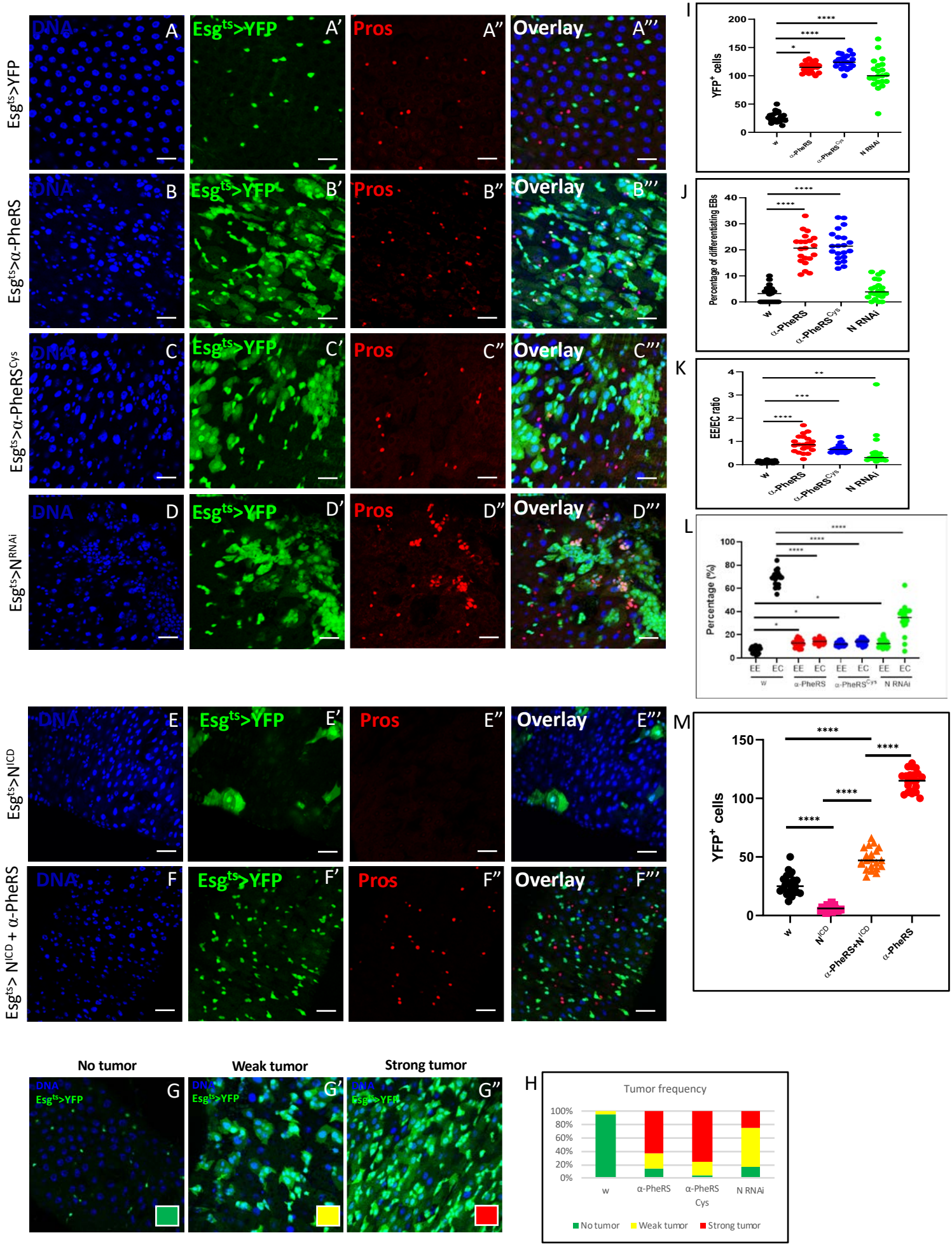
Esg^ts>YFP
Esg^ts>α-PheRS
Esg^ts>α-PheRS^Cys
Esg^ts>N^RNAi
Esg^ts>N^ICD
Esg^ts> N^ICD + α-PheRS
DNA
Esg^ts>YFP
Pros
Overlay
A
A'
A''
A'''
B
B'
B''
B'''
C
C'
C''
C'''
D
D'
D''
D'''
E
E'
E''
E'''
F
F'
F''
F'''
I
YFP+ cells
w
α-PheRS
α-PheRS^Cys
N RNAi
J
Percentage of differentiating EBs
K
EE/EC ratio
L
Percentage (%)
EE
EC
M
YFP+ cells
N^ICD
α-PheRS+N^ICD
No tumor
Weak tumor
Strong tumor
G
G'
G''
H
Tumor frequency
100%
80%
60%
40%
20%
0%
w
α-PheRS
α-PheRS Cys
N RNAi
No tumor
Weak tumor
Strong tumor

Figure 4

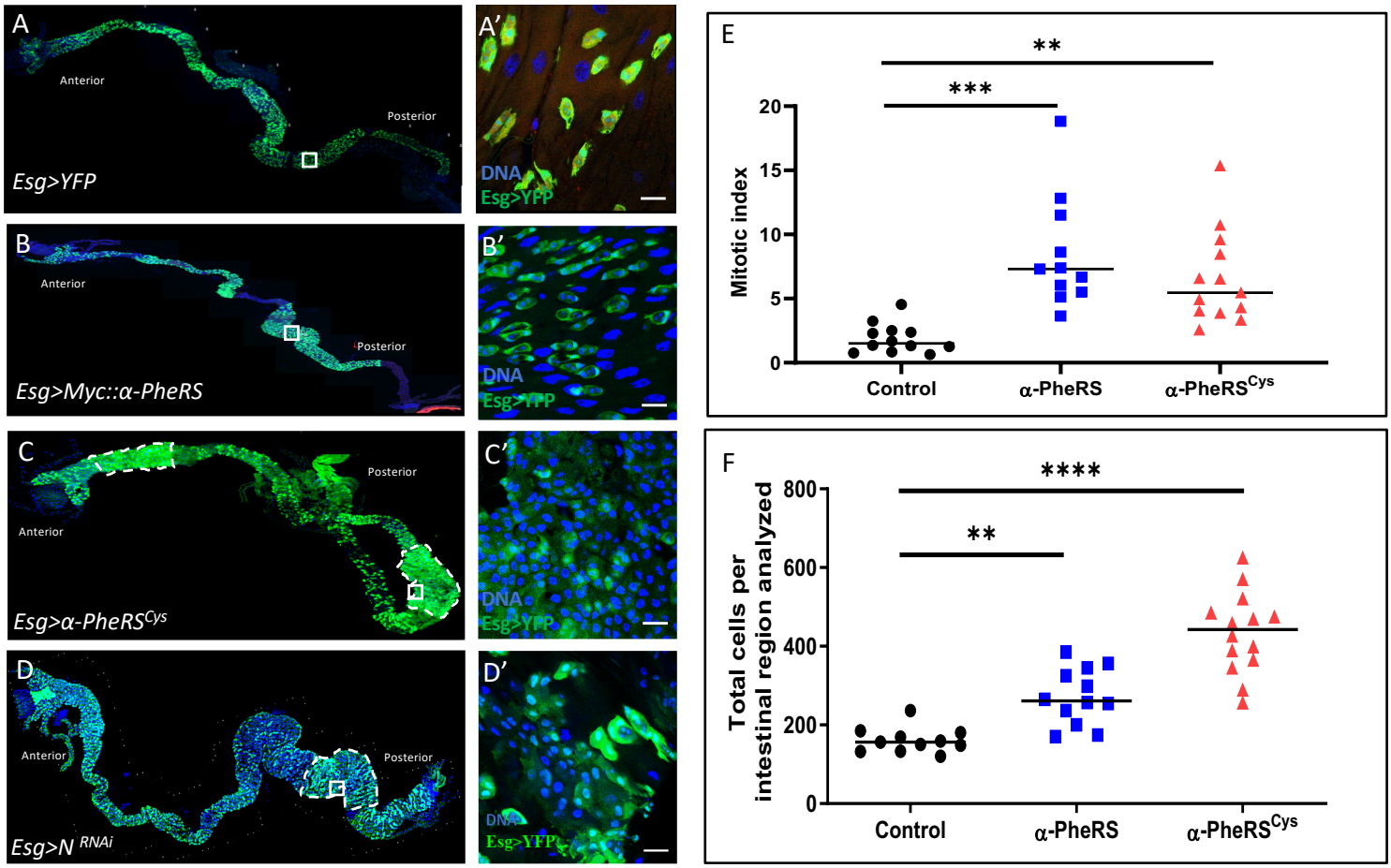
A
Anterior
Posterior
Esg>YFP
A'
DNA
Esg>YFP
B
Anterior
Posterior
Esg>Myc::α-PheRS
B'
DNA
Esg>YFP
C
Anterior
Posterior
Esg>α-PheRSCys
C'
DNA
Esg>YFP
D
Anterior
Posterior
Esg>N RNAi
D'
DNA
Esg>YFP
E
Mitotic index
0
5
10
15
20
***
**
Control
α-PheRS
α-PheRSCys
F
Total cells per intestinal region analyzed
0
200
400
600
800
****
**
Control
α-PheRS
α-PheRSCys

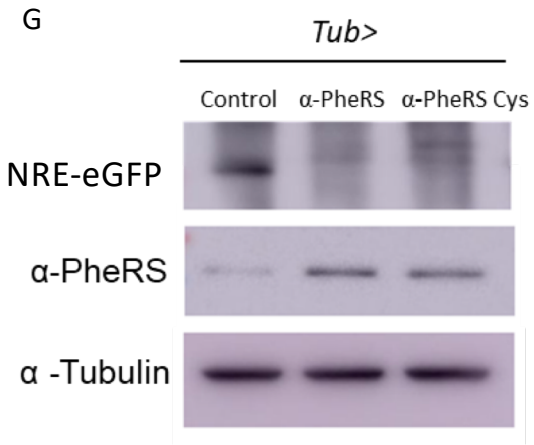
G
Tub>
Control
α-PheRS
α-PheRS Cys
NRE-eGFP
α-PheRS
α -Tubulin

Figure 5

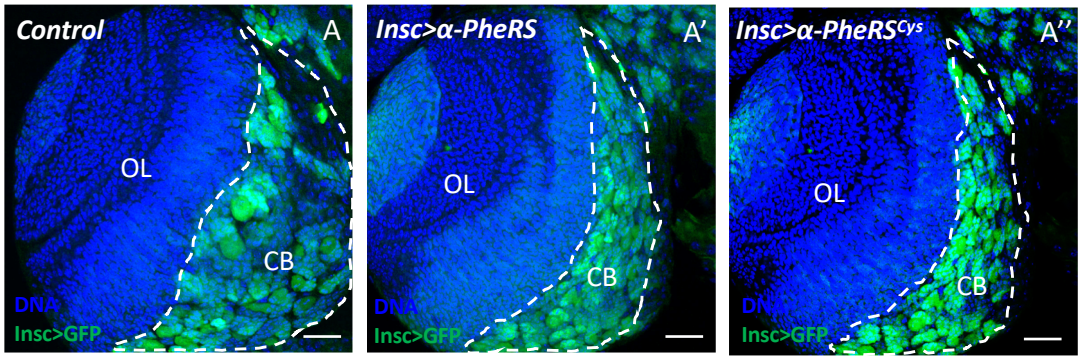
Control
A
OL
CB
DNA
Insc>GFP
Insc>α-PheRS
A'
OL
CB
DNA
Insc>GFP
Insc>α-PheRSCys
A''
OL
CB
DNA
Insc>GFP

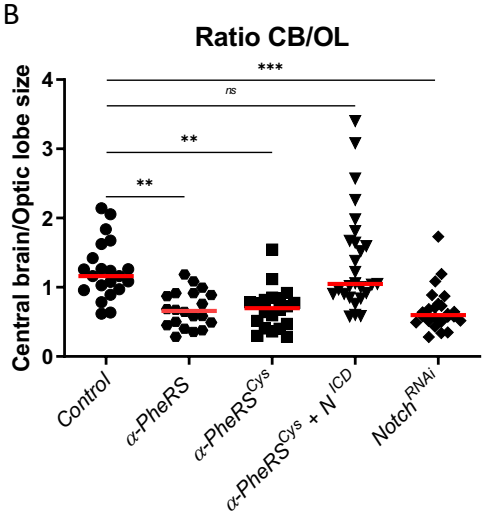
B
Ratio CB/OL
Central brain/Optic lobe size
0
1
2
3
4
***
ns
**
**
Control
α-PheRS
α-PheRSCys
α-PheRSCys + N ICD
Notch RNAi

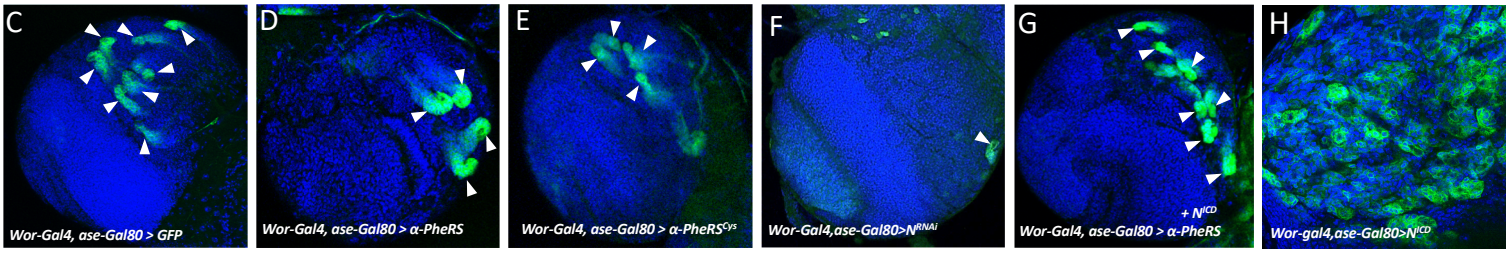
C
Wor-Gal4, ase-Gal80 > GFP
D
Wor-Gal4, ase-Gal80 > α-PheRS
E
Wor-Gal4, ase-Gal80 > α-PheRSCys
F
Wor-Gal4,ase-Gal80>NRNAi
G
+ NICD
Wor-Gal4, ase-Gal80 > α-PheRS
H
Wor-gal4,ase-Gal80>NICD

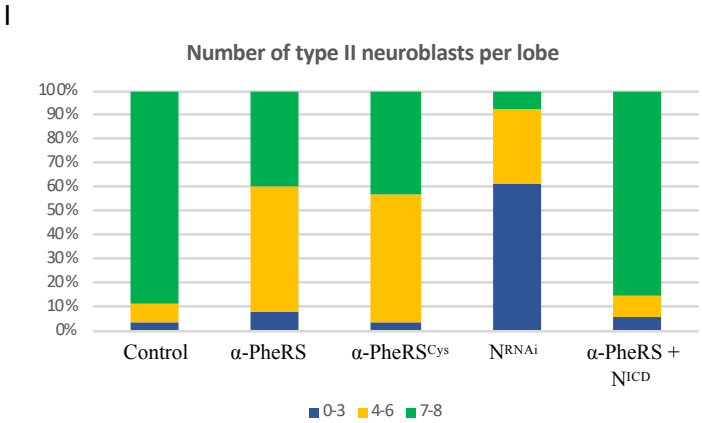
I
Number of type II neuroblasts per lobe
100%
90%
80%
70%
60%
50%
40%
30%
20%
10%
0%
Control
α-PheRS
α-PheRSCys
NRNAi
α-PheRS + NICD
0-3
4-6
7-8

Figure 6

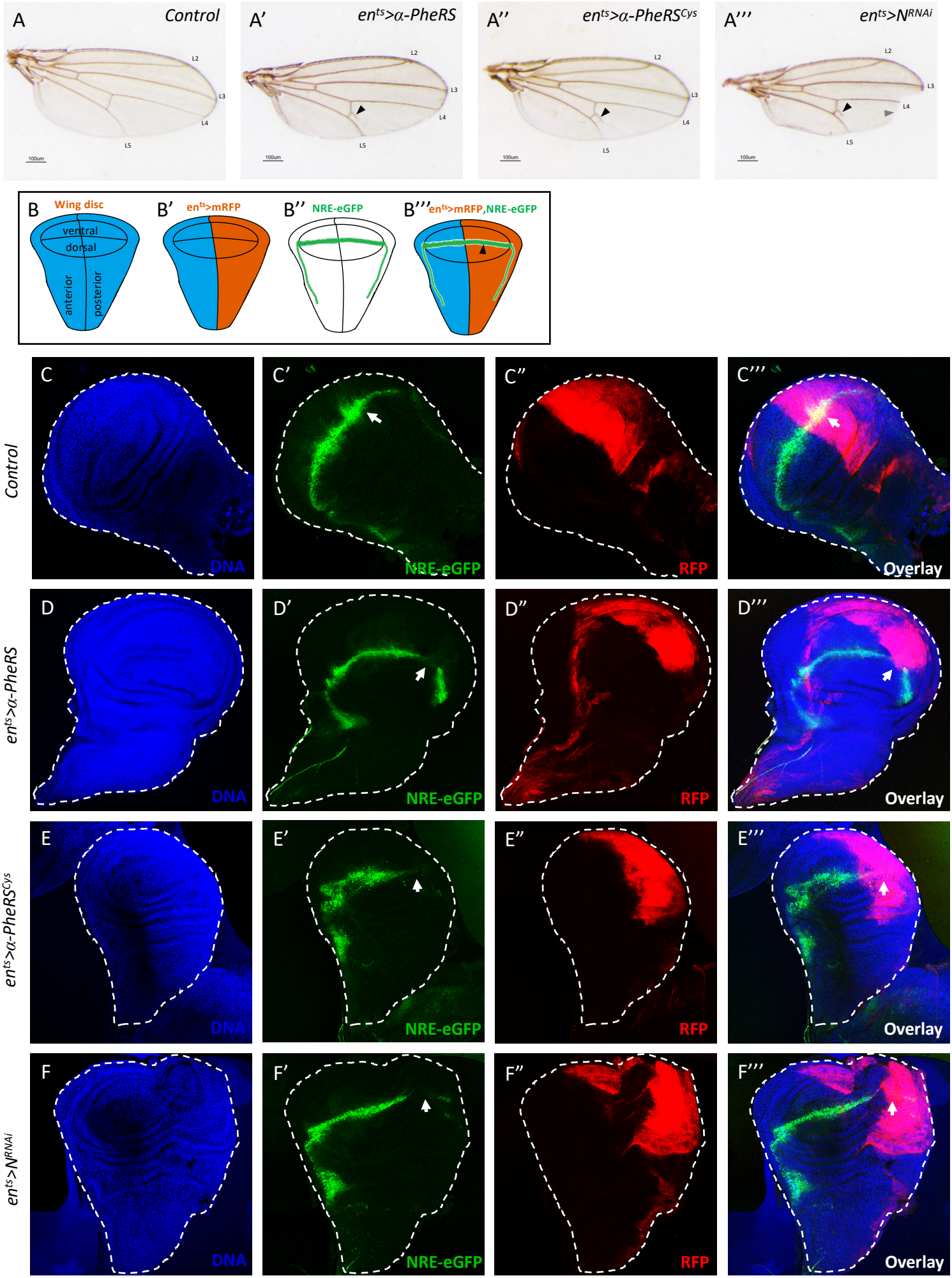
A
Control
A'
en^ts>α-PheRS
A''
en^ts>α-PheRS^Cys
A'''
en^ts>N^RNAi
L2
L3
L4
L5
100um
B
Wing disc
ventral
dorsal
anterior
posterior
B'
en^ts>mRFP
B''
NRE-eGFP
B'''
en^ts>mRFP,NRE-eGFP
Control
en^ts>α-PheRS
en^ts>α-PheRS^Cys
en^ts>N^RNAi
C
C'
C''
C'''
D
D'
D''
D'''
E
E'
E''
E'''
F
F'
F''
F'''
DNA
NRE-eGFP
RFP
Overlay

Figure 7

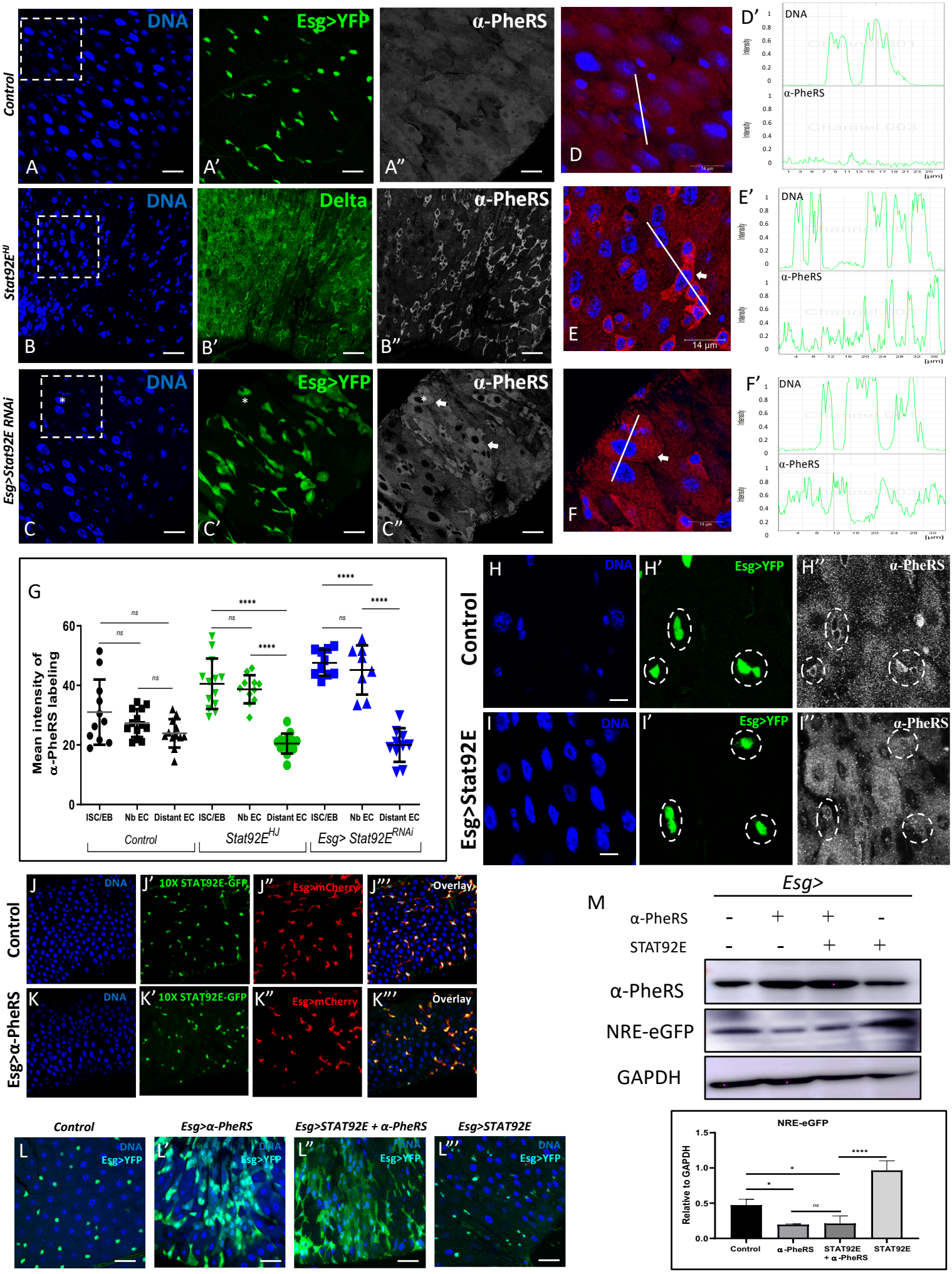
Control
Stat92E^HJ
Esg>Stat92E RNAi
DNA
Esg>YFP
α-PheRS
Delta
A
A'
A''
B
B'
B''
C
C'
C''
D
E
F
D'
E'
F'
14 µm
G
Mean intensity of α-PheRS labeling
ISC/EB
Nb EC
Distant EC
Control
Stat92E^HJ
Esg> Stat92E^RNAi
ns
****
H
H'
H''
I
I'
I''
Esg>Stat92E
J
J'
J''
J'''
K
K'
K''
K'''
10X STAT92E-GFP
Esg>mCherry
Overlay
Esg>α-PheRS
M
Esg>
α-PheRS
STAT92E
NRE-eGFP
GAPDH
Control
Esg>α-PheRS
Esg>STAT92E + α-PheRS
Esg>STAT92E
L
L'
L''
L'''
NRE-eGFP
Relative to GAPDH
Control
α-PheRS
STAT92E + α-PheRS
STAT92E